
AD 603150

APL-TDR-64-48

603150

# INVESTIGATION OF THE PARA-ORTHO SHIFT OF HYDROGEN

TECHNICAL DOCUMENTARY REPORT NO.
APL-TDR-64-48
March 1964

123 p #4.00 hc
#0.75 mf

AF Aero Propulsion Laboratory
Research and Technology Division
Air Force Systems Command
Wright-Patterson Air Force Base, Ohio

Project No. 3048, Task No. 30193

(Prepared under Contract No. AF33(657)-10333 by Air Products and Chemicals, Inc., Allentown, Pennsylvania; E. G. Biskis, J. F. Kucirka, and G. E. Schmauch (Project Leader), Authors)

## NOTICES

When Government drawings, specifications, or other data are used for any purpose other than in connection with a definitely related Government procurement operation, the United States Government thereby incurs no responsibility nor any obligation whatsoever; and the fact that the Government may have formulated, furnished, or in any way supplied the said drawings, specifications, or other data, is not to be regarded by implication or otherwise as in any manner licensing the holder or any other person or corporation, or conveying any rights or permission to manufacture, use, or sell any patented invention that may in any way be related thereto.

Qualified requesters may obtain copies of this report from the Defense Documentation Center (DDC), (Formerly ASTIA), Cameron Station, Bldg. 5, 5010 Duke Street, Alexandria 4, Virginia.

This report has been released to the Office of Technical Services, U.S. Department of Commerce, Washington 25, D.C., for sale to the general public.

Copies of this report should not be returned to the Research and Technology Division unless return is required by security considerations, contractual obligations, or notice on a specific document.

# FOREWORD

This report was prepared by Air Products and Chemicals, Inc., under USAF Contract No. AF33(657)-10333. This contract was initiated under Project No. 3048, "Aviation Fuels", Task No. 304801, "Unconventional Fuels". This work was administered by the Technical Support Division, Air Force Aero Propulsion Laboratory, Research and Technology Division, Wright-Patterson Air Force Base, Ohio, with Messrs. Herbert Lander and Perie R. Pitts, Jr. acting as project engineers.

This final report covers work conducted from November 1962 to November 1963.

The work discussed in this report was supervised by Dr. G. E. Schmauch, Manager, Contract Research, and was directed by Dr. Clyde McKinley, Director, Research and Development Department. Special thanks are due Mr. H. E. Lindenmoyer, Mr. L. Cirocco and Mr. S. W. Shurskis for their contributions to the experimental programs. The authors express their gratitude to Mrs. M. Strouse and Mrs. S. Wanish for preparing the manuscript. The authors are also grateful to Messrs. F. Kocon and D. Buss for the preparation of the many graphs and drawings.

## ABSTRACT

This report presents the results of a program for the development of catalysts for the promotion of the low temperature para-ortho reaction of hydrogen. This program has resulted in the preparation and testing of a catalyst with an activity 13.7 times greater on a weight basis than the best commercial material. Detailed mechanism studies have resulted in a model for the conversion reaction which successfully predicts the kinetic behavior over a wide range of flow rate, pressure, and catalyst particle size. Catalyst poisoning studies have further elucidated the reaction mechanism, and indicate a rate reduction probably due to the blocking of the mouths of the catalyst pores.

This technical documentary report has been reviewed and is approved.

Marc P. Dunnam

MARC P. DUNNAM
Chief, Technical Support Division
AF Aero Propulsion Laboratory

# TABLE OF CONTENTS

## TABLE OF CONTENTS (Cont'd)

## LIST OF FIGURES

## LIST OF FIGURES (Cont'd.)

## LIST OF TABLES

# I. INTRODUCTION

A program has been conducted for the purpose of developing highly active catalysts for promoting the low temperature para-ortho reaction of hydrogen. An earlier program had produced a catalyst with about 9.7 times the activity of the best commercial material, on a weight basis. The present program has succeeded in raising this activity from 9.7 to 13.7.

These advances were achieved through a systematic study of the preparational variables of the catalyst, and through a series of qualitative mechanism studies. The mechanism studies have included investigation of the following limitations to conversion rate: diffusion of reactant and product to and from the bulk gas to the catalyst surface; diffusion of reactant and product into and out of the catalyst pores; adsorption and desorption of the reactant and product at the catalyst surface; and surface reaction. The results of the mechanism studies point the way towards further potential improvement of the present catalyst system, and provide the tools for more systematic investigation of other catalyst systems for this reaction.

Manuscript released by authors March 1964 for publication as a Technical Documentary Report.

## II. DETERMINATION OF RATE LIMITATIONS

Since the advent of the Air Products' investigation of the para-ortho shift of hydrogen, a continual effort has been made to define the over-all mechanism of conversion. The complexity of this analysis becomes apparent if one remembers that the conversion of a gaseous reactant in the presence of a solid catalyst consists of a series of seven sequential steps:

1. Transport of the reactant from the bulk gas phase to the external surface of the catalyst.

2. If the catalyst is porous, movement of the reactant through the internal pores.

3. Adsorption of the reactant on the catalyst surface.

4. A chemical reaction on the catalyst surface.

5. Desorption of the product.

6. Diffusion of the product through the pores to the external surface.

7. Transport of the product from the interface to the bulk gas stream.

The steps of the sequence which proceed at the slowest rates will limit the over-all rate of conversion and will therefore be the "conversion bottlenecks". The physical and chemical characteristics of the catalyst, and the conditions of reactor operation will determine the relative importance of these steps. Consequently, knowledge of the controlling factors in the process is mandatory in a scientific study and optimization of catalysts.

Air Products and Chemicals, Inc. determined these ortho-para hydrogen conversion rate limitations with a program of planned theoretical analyses supplemented by specific experimentation. In this manner, the economic inefficiencies caused by theory impasses were minimized and intermediate results were of utility in the APACHI Catalyst Development Program. In addition to their specific application in the Air Products' study, the general results are applicable to any scheme of ortho-para hydrogen catalytic conversion which may be of interest to the Air Force.

The theoretical analyses of the rate limitation contributions of each of these steps, the results of coordinated experimentation, and the interpretation of these theoretical results in light of the experimental data will be presented in that order.

In summary, Air Products and Chemicals, Inc., concluded that the combined resistances of bulk diffusion, pore diffusion, and surface reaction limited the catalytic conversion of ortho to parahydrogen.

## A. THEORETICAL ANALYSES

An exact solution of the over-all rate, which consists of seven rates in series, is extremely complex. The initial attempt was to analyze each step independently, with the assumption that the step in question was rate-controlling and that all other resistances to conversion were relatively minor. From these theoretical results, predictions of the effects of catalyst pore size distribution, particle size, gas flow rate, and pressure on the kinetic rates of these steps were made prior to the experimentation.

In a study of a steady state, equimolar conversion such as the para to ortho transition, the number of conversion steps which must be analysed are reduced. The rate of diffusion of the reactant from the bulk gas phase to the external surface of the catalyst must equal the rate of transport of the product away from this interface. Correspondingly, the rates of pore diffusion of both the reactant and product must be identical. Thus a complete analysis of mechanism can be obtained by studies of the following steps:

1. Transport of the orthohydrogen from the bulk gas stream to the external surface of the catalyst.

2. If the catalyst is porous, diffusion of the orthohydrogen through the internal pores.

3. Adsorption of the orthohydrogen on the catalyst surface.

4. Ortho to parahydrogen conversion on the catalyst surface.

5. Desorption of the parahydrogen.

Although the primary objective of this contract was to study the para to ortho transition of hydrogen, the basis of the analysis of mechanism was the ortho to para conversion. The results of any study concerning the one conversion is thermodynamically related to the other. For the first order reversible conversion of ortho to para hydrogen:

$$\text{ortho } H_2 \underset{\text{reverse}}{\overset{\text{forward}}{\rightleftharpoons}} \text{para } H_2$$

$$\text{Forward rate} = k_f \, (O\text{-}H_2)$$

$$\text{Reverse rate} = k_R \, (P\text{-}H_2)$$

At equilibrium,

$$\text{Forward rate} = \text{Reverse rate}$$

$$k_F \, (O\text{-}H_2)_e = k_R \, (p\text{-}H_2)_e$$

$$\frac{(p\text{-}H_2)_e}{(O\text{-}H_2)_e} = \frac{k_F}{k_R} = K = \text{Thermodynamic equilibrium constant}$$

Since the equilibrium constant is known as a function of temperature, a determination of the forward reaction rate constant at any temperature automatically leads to an anlysis of the reverse reaction at that temperature. Experimentally, it was more economical to study the ortho to para hydrogen transition, and this conversion became the basis of the mechanism analysis.

1. Bulk Diffusion

Bulk diffusion is the migration of the reactant from the flowing gas stream, through the laminar boundary layer surrounding each catalyst particle, to the external surface of the catalyst. The thickness of this boundary layer and hence the rate of diffusion through it is a function of the linear velocity, viscosity, and density of the gas; the diffusivity and concentration of the migrating species;

the pressure of the system; the cross sectional area of the reactor; and the catalyst particle size. Since the variables are numerous, the development of a theoretical analysis of the effect of bulk diffusion was lengthy and is presented in Appendix I. The results and interpretation of this analysis will be considered in this section.

In a packed bed tubular reactor where bulk diffusion limits the over-all rate of conversion, the mathematical relationship between the observed rate of reaction and the reactant concentration log mean driving force would be as follows:

$$R_r = \frac{F}{W}(y_1 - y_2) = k_B \frac{LMDF}{1 - 1/2(LMDF) - 1/2\left[\frac{y_e}{\ln\left(\frac{y_1 - y_e}{y_2 - y_e}\right)}\right]} \quad (1)$$

where $R_r$ = Observed rate of conversion, gram moles/sec· gram cat.

$y_1$ = orthohydrogen mole fraction in the reactor inlet stream

$y_2$ = orthohydrogen mole fraction in the reactor outlet stream

$y_e$ = thermodynamic equilibrium mole fraction of orthohydrogen at a given temperature

$F$ = molar flow rate of hydrogen in the reactor, gram moles/sec·

$W$ = mass of catalyst in the reactor, grams

LMDF = log mean driving force, $\frac{y_1 - y_2}{\ln[(y_1 - y_e)/(y_2 - y_e)]}$

$k_B$ = bulk mass transfer coefficient, $\frac{\text{gm moles } H_2 \text{ converted}}{\text{sec x gram catalyst}}$

If the temperature of the system is constant, the bulk mass transfer coefficient, $k_B$, is related to the variables which control the thickness of the diffusion boundary layer in the following manner:

$$k_B = (\text{constant})\ (G)\ (d_p)^{-1.51}\ (\mu)^{-0.15} \qquad (2)$$

where

G = superficial molar flow rate of hydrogen per unit cross sectional area of the reactor, $\frac{\text{gram moles } H_2}{\text{sec x cm}^2 \text{ empty reactor}}$

$d_p$ = catalyst particle diameter, cm

$\mu$ = viscosity of hydrogen at T and P of reactor, poise

In a packed bed, tubular reactor of the type utilized by Air Products and Chemicals, Inc. in the study of para-ortho hydrogen conversion, an increase in hydrogen flow rate causes an increase in the log mean driving force of the system. If bulk mass transfer were to limit the over-all conversion, equation (2) predicts that the bulk mass transfer coefficient would also increase.

Thus if the diffusion of ortho hydrogen from the bulk gas stream to the external surface of the catalyst were to limit the over-all rate of conversion, equation (1) and (2) predict that the dependency of the observed reaction rate on the log mean driving force would be greater than a direct proportionality. Figure 1 is a graphical presentation of this prediction.

The only variable in equation (2) which is affected by pressure is the viscosity of hydrogen at the reactor conditions. However, the pressure dependency is very weak: $k_B$ is proportional to $(\mu)^{-0.15}$, where $\mu$ is a function of pressure. For example, at -320°F, the viscosity of hydrogen is 0.009 and 0.0116 lb. mass per foot per hour at pressures of 100 and 1500 pounds per square inch gauge, respectively. Consequently, the bulk mass transfer

coefficient at 1500 psig would be only 4% larger than $k_B$ at 100 psig. If bulk mass transfer were to limit the overall rate of conversion, an increase in reaction rate of only 4% would be expected at 1500 psig relative to 100 psig.

Since the flow conditions and therefore the laminar boundary layer are very dependent on the catalyst particle external characteristics, the bulk mass transfer coefficient would be expected to be dependent on these characteristics. Equation (2) illustrates this dependency; the bulk mass transfer is a function of the -1.51 power of the particle diameter. Thus, if bulk mass transfer were the only limitation, the rate of reaction should increase by a factor of eight when the catalyst particle size is decreased from 20-25 to 80-100 mesh.

The internal pore characteristics of the catalyst do not affect the external boundary layer. Consequently, bulk mass transfer is independent of the pore size distribution.

In summary, then, if the conversion rate is controlled by bulk diffusion, the following would be expected:

(1) The second derivative of the conversion rate - log mean driving force curve would be positive (that is, the slope of the curve will continually increase).

(2) The effect of pressure on the conversion rate would be negligible.

(3) A factor of 8 improvement in conversion rate would result as particle size is reduced from 20-25 mesh to 80-100 mesh.

(4) The conversion rate would be independent of pore size distribution.

2. Pore Diffusion

Pore diffusion is the migration of the reactant from the external surface of the catalyst, through the catalyst pores, to the interior surface. The rate of pore diffusion is a function of the temperature; pressure; molecular diffusivity and concentration of the reactant; the rate of surface reaction; and the pore size distribution and surface area of the catalyst.

The beginning of a derivation of this relationship for pore diffusion is a steady state orthohydrogen material balance on a differential element dx of a catalyst pore of radius r:

| Rate of ortho-hydrogen into a pore segment dx in length | - | Rate of ortho-hydrogen out | - | Rate of ortho-hydrogen conversion on the walls of the pore segment | = 0 |
|---|---|---|---|---|---|

The result of this balance is:

$$D\,r\,\frac{d^2y}{dx^2} = 2\,k_f\,y - \frac{2\,k_f}{K}\,(1 - y) \qquad (3)$$

where

D = orthohydrogen diffusivity within the pore, $cm^2/sec$

r = pore radius, cm

x = pore length, cm

y = orthohydrogen mole fraction

K = ortho-parahydrogen equilium constant

$k_f$ = ortho to parahydrogen reaction rate constant, $cm^3/sec \times cm^2$

Equation 3, the beginning of a theoretical pore diffusion analysis which is presented in detail in Appendix II, immediately indicates that a pore diffusion analysis must include the effects of surface reaction. In brief, the conversion of ortho to parahydrogen on the surface of a pore increases the orthohydrogen concentration gradient within the pore and thus increases the rate of diffusion. Consequently, an analysis of pore diffusion must include the effects of surface reaction.

The end result of the analysis of pore diffusion limitation was the following expression relating the observed reaction rate and the reactant concentration logarithmic mean driving force:

$$R_r = \frac{F}{W}(y_1 - y_2) = E_p k_f (LMDF) \qquad (4)$$

where

$R_r$ = observed rate of conversion, gram moles/sec · gram cat.

$y_1$ = orthohydrogen mole fraction in the reactor inlet stream

$y_2$ = orthohydrogen mole fraction in the reactor outlet stream

$y_e$ = thermodynamic equilibrium mole fraction of orthohydrogen at a given temperature.

$F$ = molar flow rate of hydrogen in the reactor, gram moles/ sec·

$W$ = mass of catalyst in the reactor, grams

LMDF = log mean driving force, $\dfrac{y_1 - y_2}{\ln[(y_1-y_e)/(y_2-y_e)]}$

$k_f$ = ortho to parahydrogen reaction rate constant, gm moles/ gm cat x sec

$E_p$ = pore effectiveness factor

= $\dfrac{\text{actual reaction rate limited by pore diffusion}}{\text{ideal reaction rate when pore diffusional resistance is zero}}$

The pore effectiveness factor, $E_p$, is a direct measure of the pore diffusion resistance. When $E_p$ is equal to 1.0, no pore diffusional resistance exists; when pore diffusional limitations are present, $E_p$ is less than 1.0. The effectiveness factor is related to the physical and chemical properties of the reactant and catalyst in the following manner:

$$E_p = 3\left[\frac{(h \coth h) - 1}{h^2}\right] \qquad (5)$$

where

$$h = \frac{d_p}{2}\sqrt{\frac{k_f \rho_p RT}{D_p P}} \qquad (6)$$

$d_p$ = catalyst particle diameter, cm

$D_p$ = effective diffusivity within the porous catalyst, $cm^2/sec$

$\rho_p$ = catalyst particle density, $gm/cm^3$

T = temperature, °K

P = pressure, atm.

R = gas constant, $\frac{atm \times cm^3}{gm\ moles \times °K}$

In the section entitled "Surface Reaction", it will be shown that $k_f$ is directly proportional to the system pressure. Combining this fact with equations 4, 5 and 6 leads to the conclusion that the observed conversion rate would be approximately directly proportional to the system pressure if the only limitation were pore diffusion.

Since the migration of orthohydrogen through the pores of a catalyst is independent of the gas flow rate outside of the porous pellet, the observed reaction rate where pore diffusion is the limitation should be independent of flow conditions. Thus, the observed reaction rate, according to equation 4, should be directly proportional to the log mean driving force. Figure 1 illustrates this dependency.

The catalyst physical properties affect the reactants effective diffusivity and consequently a dependency of observed reaction rate on the catalyst pore size distribution, surface area, and particle diameter would be expected.

In summary, a conversion rate controlled by pore diffusion would have the following characteristics:

(1) The conversion rate would be directly proportional to the pressure.

(2) The conversion rate would be independent of the hydrogen flow rate.

(3) The conversion rate would be directly proportional to the log mean driving force.

(4) The conversion rate would be dependent on the catalyst pore size distribution, surface area, and pore size distribution.

3. Adsorption and Desorption

The possibility that adsorption of the reactant or desorption of the product controlled the over-all rate of conversion was explored by using an approach modeled after that developed by Langmuir ( 1 ). Several assumptions are pertinent to this treatment:

a. All the surface of the catalyst has the same activity for adsorption.

b. A monomolecular layer of adsorbent or less is present.

c. All the adsorption occurs by the same mechanism.

Since the adsorption is limited to a monomolecular layer, the surface may be divided into two parts, the fraction $\Theta$ covered by the monomolecular layer of adsorbed molecules and the fraction $(1-\Theta)$ which is bare. Since only molecules striking the uncovered part of the surface can be adsorbed, the rate of adsorption per unit total area will be proportional to $1 - \Theta$. Thus

$$r_a = k_a y P (1-\Theta) \qquad (7)$$

where

$r_a$ = rate of adsorption, $\frac{\text{gm moles}}{\text{gm cat x sec}}$

$k_a$ = specific adsorption rate coefficient, $\frac{\text{gm moles}}{\text{atm x sec x gm cat}}$

$P$ = total pressure, atm

$y$ = orthohydrogen mole fraction in the gas.

If the surface conversion of ortho to parahydrogen were instantaneous, the desorption rate of parahydrogen would be:

$$r_d = k_d \Theta \qquad (8)$$

where

$r_d$ = desorption rate of parahydrogen, $\frac{\text{gm moles}}{\text{sec x gm cat}}$

$k_d$ = specific desorption rate coefficient, $\frac{\text{gm moles}}{\text{sec x gm cat}}$

For monomolecular layer adsorption, the fraction covered is proportional to the volume of gas adsorbed.

$\Theta$ = (constant) $V = CV$

where

$V$ = Volume of hydrogen adsorbed, $cm^3/gm$ cat
= some function of pressure, $f(P)$

Thus

$$r_a = k_a P_y \left(1 - f(P)\right) \qquad (9)$$

and

$$r_d = k_d f(P) \qquad (10)$$

The specific adsorption rate constants, $k_a$ and $k_d$, are functions of the chemical properties of the catalyst, reactant, product, and the system temperature. Any postulation concerning the effect of pressure at any temperature is highly dependent on the adsorption isotherm, f(P).

It can be seen from equation 8 and 9 that the observed rate of reaction would be independent of gas flow rate, and the catalyst physical characteristics (with the exception of surface area) if either adsorption of the reactant or desorption of the product, controlled the over-all conversion.

4. Surface Reaction

Previous investigators (3) have determined that the ortho-parahydrogen conversion can be interpreted as a first order, reversible reaction:

$$O - H_2 \rightleftharpoons p - H_2$$

and

$$\frac{-dC_o}{dt} = k_f C_o - k_r C_p$$

$$\frac{-dC_o}{dt} = k_f C_o - \frac{k_f}{K} C_p \qquad (11)$$

where

$C_o$ = concentration of orthohydrogen, $\frac{\text{gm moles}}{\text{cm}^3}$

$C_p$ = concentration of parahydrogen, $\frac{\text{gm moles}}{\text{cm}^3}$

$t$ = time, sec

$k_f$ = forward reaction rate constant, $\text{sec}^{-1}$

$k_r$ = reverse reaction rate constant, $\text{sec}^{-1}$

$K = \frac{k_f}{k_r}$ = thermodynamic equilibrium constant

$\frac{dC_o}{dt}$ = net rate of conversion of ortho to para hydrogen, $\frac{\text{gm moles}}{\text{sec x cm}^3 \text{ bed}}$

By converting the concentration terms in equation 11 to mole fractions and applying a material balance over a differential segment of catalyst bed, an expression, in terms of the reactor inlet and outlet ortho hydrogen concentrations, for the observed reaction rate is obtained for the case when the surface reaction controls the overall rate. The mechanics of derivation are identical to those presented in Appendix I for bulk diffusion, and will not be presented here.

$$R_r = \frac{F}{W}(y_1 - y_2) = k_f (LMDF) \qquad (12)$$

where

$R_r$ = observed rate of conversion, $\frac{\text{gm moles}}{\text{sec} \cdot \text{ gm cat.}}$

$F$ = molar flow rate of $H_2$ $\frac{\text{gm. moles}}{\text{sec}}$

$W$ = mass of catalyst in system, grams

$k_f$ = specific reaction rate constant, $\frac{\text{gm moles}}{\text{sec x gm cat}}$

= (constant) x P at temperature T for a particular catalyst

$P$ = absolute pressure, atmospheres

$T$ = absolute temperature, °K

LMDF = log mean driving force,

$$(y_1 - y_2)/\ln\left[(y_1 - y_e)/(y_2 - y_e)\right]$$

$y_1$ = reactor inlet orthohydrogen in mole fraction

$y_2$ = reactor outlet orthohydrogen mole fraction

$y_e$ = thermodynamic equilibrium orthohydrogen mole fraction at temperature T

For a surface reaction rate controlling situation, equation 12 predicts that the observed reaction rate will be directly proportional to the log mean driving force, and the absolute pressure of the system. However, it will be independent of the conditions of flow within the reactor, and the particle size and pore size distribution of the catalyst.

The reaction rate constant, $k_f$, is in terms of catalyst mass for a specific catalyst system. Consequently, if the chemical structure of the catalyst were kept constant, and its surface area per unit mass were increased, the reaction rate constant and thus the observed reaction rate would increase proportionately.

5. Bulk Diffusion, Pore Diffusion, and Surface Reaction Combined Limitation

Instead of one limitation, a reaction system may have a combination of two or more limitations, all of the same order of magnitude. The combined resistance then becomes a complex function of all of the variables which influence each of the elements of the combination. Consequently, the theoretical analysis and experimental verfication of such a reaction system become complicated. An example of such a situation is the case where a combined influence of bulk diffusion, pore diffusion, and surface reaction is important.

The constant catalyst mass flow reactor utilized by Air Products in the ortho-parahydrogen conversion studies was designed for operation with lower activity catalysts such as ferric oxide gel. For a catalyst of this type, the effects of bulk diffusion are usually negligible and thus the gas flow in the reactor need not be turbulent. However, with the advent of the high activity APACHI catalysts, a re-evaluation of the flow situation revealed that the measure of reactor turbulance, the Reynold's number, ranged from 9 to 46 and the flow was therefore laminar in nature. In reactor applications, the Reynold's number is defined as follows:

$$Re = \frac{d_p \rho v}{\mu}$$

where

$d_p$ = catalyst particle diameter, cm

$\rho$ = gas density, $gm/cm^3$

v = superficial gas velocity in the reactor, cm/sec

$\mu$ = gas viscosity, poise

For the constant mass ortho-parahydrogen reactor, the Reynold's number increased with an increase in the concentration log mean driving force. Thus since the flow in the reactor was laminar, the possibility existed that bulk diffusion could control the process at low values of LMDF and the combination of pore diffusion and surface reaction could limit the conversion at higher values of LMDF.

On the basis of this possibility, the effects of a combined influence of bulk diffusion, pore diffusion, and surface reaction were theoretically analyzed. The result was the following relationship between the observed reaction rate and the concentration log mean driving force.

$$R_r = \frac{F}{W} (y_1 - y_2) = k E_B E_P (LMDF) \qquad (13)$$

where

$R_r = \frac{\text{gram moles}}{\text{sec x gm catalyst}}$, observed rate of conversion

F = hydrogen flow rate, gram moles/sec

W = mass of catalyst in system, grams

LMDF = log mean driving force, $(y_1-y_2)/\ln\left[(y_1-y_e)/(y_2-y_e)\right]$

$y_1$ = reactor inlet orthohydrogen mole fraction

$y_2$ = reactor outlet orthohydrogen mole fraction

$y_e$ = thermodynamic equilibrium mole fraction of orthohydrogen at the system temperature.

k = specific reaction rate constant, gm-moles/sec x gram catalyst.

= function of temperature; pressure; chemical and physical properties of the catalyst.

$E_B$ = bulk diffusion effectiveness factor, $E_B = 1$ when no bulk diffusion limitation; $E_B < 1$ when limitation is present.

= function of temperature; catalyst particle size; gas flow rate; reactor diameter; viscosity, diffusivity, and density of the gas.

$E_P$ = pore diffusion effectiveness factor. $E_P = 1$ when no pore diffusion limitation; $E_P < 1$ when limitation is present.

= function of temperature; pressure; catalyst particle size, pore size distribution, and surface area; the reactant diffusivity; and the specific reaction rate constant of the system.

The many terms alone adequately depict the complexity of forming quantitative postulations as to the effects of variables. However, as it was stated before, bulk diffusion would probably limit the process at low LMDF values, and the resistances of pore diffusion and surface reaction would probably limit the process at low LMDF values, and the resistances of pore diffusion and surface reaction would probably be controlling at high values of LMDF. Thus the postulations presented in the sections entitled "Bulk Diffusion" and "Pore Diffusion", and graphically illustrated in Figure 1, would indicate that the relationship of reaction rate and LMDF should be similar to Figure 2 if the combination of resistances were decisive.

The same is true for all other variable effect postulations. If one of the three limitations is predominate under given

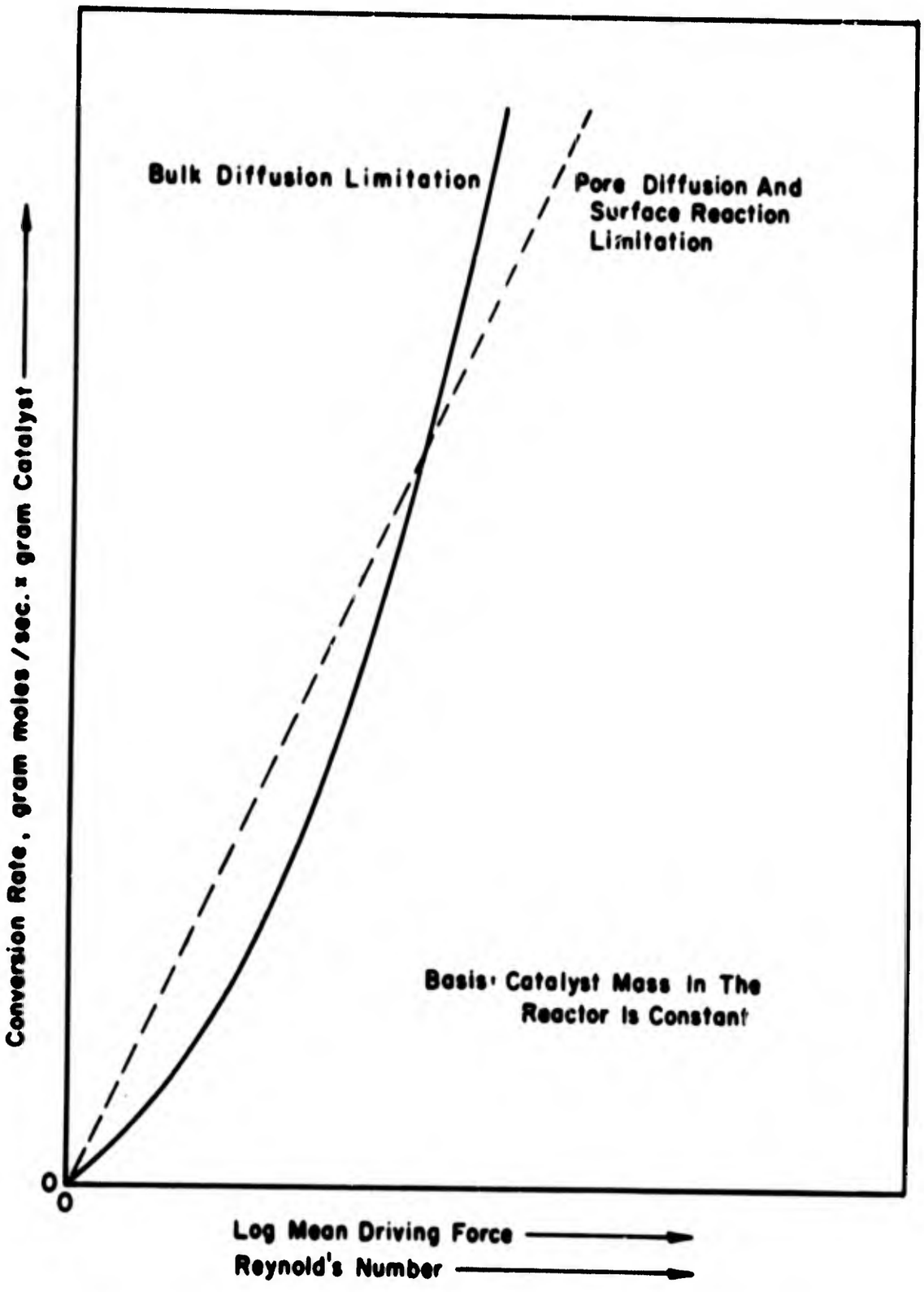


Figure 1. Conversion Rate Versus Log Mean Driving Force

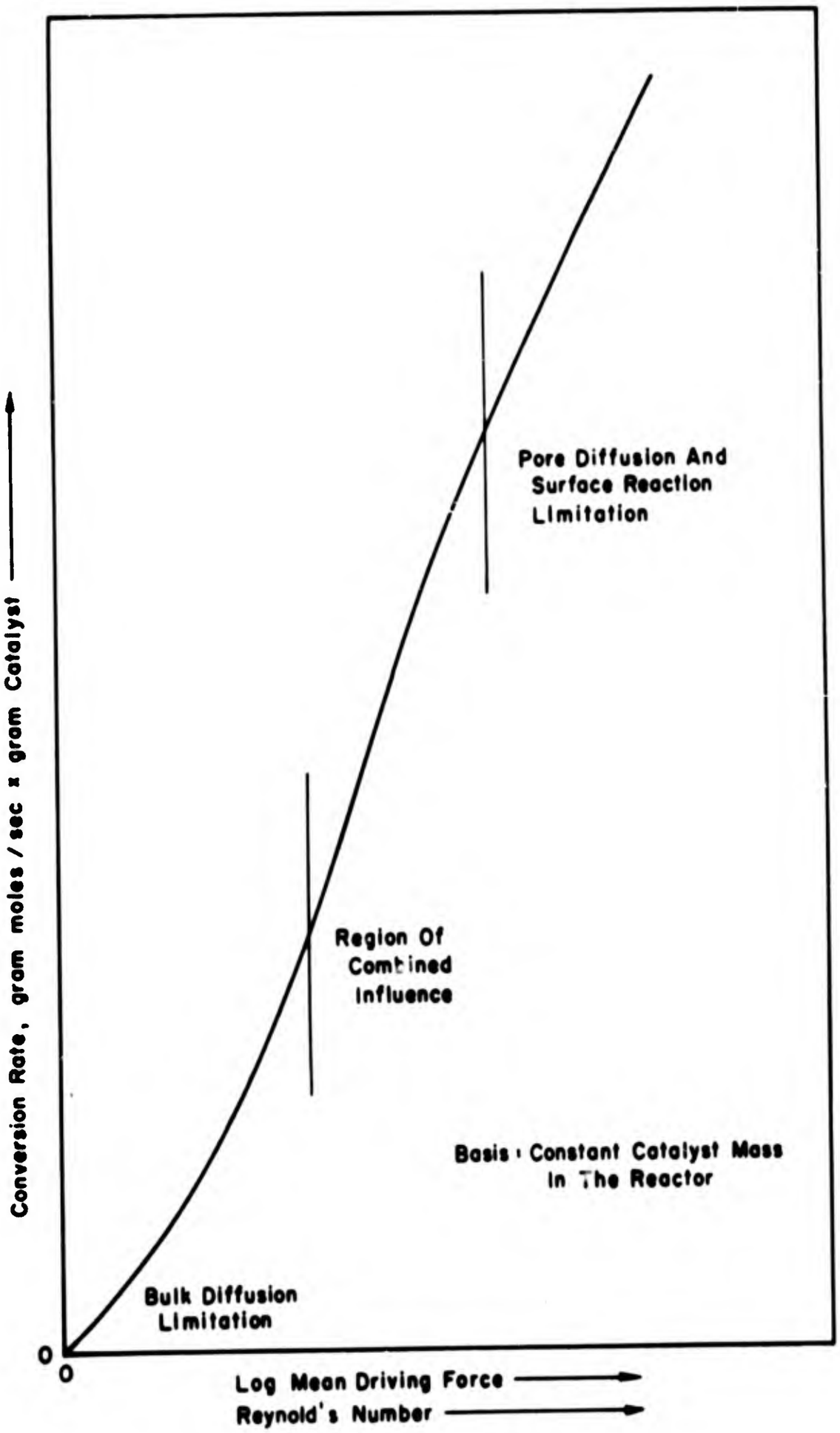


Figure 2. Conversion Rate Versus Log Mean Driving Force

conditions of operation, the effects of all variables will be similar to the effects of the variables on the dominating limitation alone. If all three limitations are important, the resultant effect will be a hybrid.

For example, consider the effect of pressure. The rates of pore diffusion and surface reaction are approximately directly proportional to pressure; but the rate of bulk diffusion is only a weak function of pressure. Consequently, the relative importance of bulk diffusion to the other two increases with an increase in pressure, and finally, at a sufficiently high pressure, bulk diffusion alone should control the conversion process.

## B. EXPERIMENTAL VERIFICATION OF ANALYSES

Although the effects of bulk diffusion, pore diffusion, adsorption, desorption, and surface reaction were ascertained theoretically, the application of these results to a specific reactant-catalyst system is not possible without knowledge of the important chemical and physical properties of the system. On this basis, a series of selected experiments were designed and performed to provide data with which the theoretical analyses could be evaluated to determine the controlling resistances.

### 1. Catalyst Physical and Chemical Properties

Since the complete characterization of all of the APACHI catalysts prepared to date was an economic impossibility, a representative group were chosen and evaluated. This group consisted of samples of Cryenco ferric oxide gel, the standard basis of comparison in orth-parahydrogen studies; APACHI 1049, which was used in the rate limitation verification experiments; APACHI 1070-95, the highest activity catalyst produced to the date of the catalyst characterizations; and APACHI 1070-82, a relatively low activity catalyst. In this manner, the chemical and physical differences in these catalysts were determined and this data helped to explain the differences in their catalytic activities.

The chemical and physical characteristics and the standard analytical techniques employed were as follows:

a. Surface area: the standard Brunauer-Emmett-Teller (BET) technique.

b. Moisture loss upon drying at 150° and 250°C.

c. Pore volume and size distribution: mercury porosimeter technique.

d. Weight loss due to ignition.

e. Metal and alkali oxide content: J. Lawrence Smith wet chemical analysis.

The results of these analyses are presented in Tables I and II, and Figures 3 through 6.

These data immediately answer several important questions. The chemical compositions presented in Table 1 show that the 1070-82 had a significantly lower metal oxide content than either the 1049-100 or 1070-95; consequently, the reason for the significantly lower activity of 1070-82 is apparent.

APACHI 1049-100 and 1070-95 have very similar chemical compositions, surface areas, and pore size distributions. However on the wet basis used in the catalyst activity studies, 1070-95 has a slightly higher activity than 1049-100. Table I shows that the moisture content of 1049-100 is higher than that for 1070-95. Consequently, on a dry basis, it can be seen that both would have about the same activity as the remainder of the catalyst characterization data predict.

Figures 3 through 6 present the pore size distribution data. It can be seen that the ferric oxide gel has only a micropore structure, with an average pore radius of about 22 A°. On the other hand, the APACHI catalysts have both a micropore (average radius of approximately 18°A). A study of the APACHI preparation technique revealed that this result was to be expected.

As a cross check of the results, the average pore sizes were calculated using the total pore volume in the pores smaller than 350°A in radius and the total BET surface area, with the assumptions that all of the surface area is in pores smaller than 350°A in radius, and the pores are cylindrical in structure. The calculation was performed in the following manner:

TABLE 1

CATALYST SURFACE AREA, MOISTURE AND IGNITION LOSSES, AND CHEMICAL COMPOSITION

| Catalyst | Surface Area After Drying at T, square meters per gram | | Moisture Loss Due to Drying at T, weight per cent | | Ignition Loss Before Drying weight per cent | Chemical Composition (Ignited Basis) | |
|---|---|---|---|---|---|---|---|
| | 150° C | 250° C | 150° C | 250° C | | $Na_2O$ Wt % | Metal Oxide Wt % |
| APACHI 1049-100 | 562 | 561 | 14.2 | 16.3 | 20.12 | 0.01 | 32.72 |
| APACHI 1070-82 | 449 | 452 | 8.4 | 10.8 | 14.60 | 0.84 $\pm$ 0.06 | 25.0 |
| APACHI 1070-95 | 669 | 587 | 10.0 | 11.4 | 15.99 | 0.02 | 32.98 |
| Cryenco Ferric Oxide Gel | 256 | 231 | 9.5 | 11.6 | - - - | - - - | - - - |

TABLE 2

CATALYST PORE VOLUME DISTRIBUTION

| Porosimeter Pressure (psia) | Pore Diameter in Microns | APACHI 1049-100 Pumped at 150°C | | APACHI 1070-82 Pumped at 150°C | | APACHI 1070-95 Pumped at 150°C | | APACHI 1070-95 Pumped at 250°C | | Cryenco Ferric Oxide Gel Pumped at 150°C | |
|---|---|---|---|---|---|---|---|---|---|---|---|
| | | V | ΔV | V | ΔV | V | ΔV | V | ΔV | V | ΔV |
| 0.45 | 22.0 | 0 | - | 0 | - | 0 | - | 0 | - | 0 | - |
| 4.9 | 14.6 | .042 | .042 | .046 | .046 | .035 | .035 | .041 | .041 | .023 | .023 |
| 9.8 | 10.3 | .062 | .020 | .062 | .016 | | | | | .032 | .009 |
| 14.7 | 8.0 | .069 | .007 | .072 | .010 | .056 | .021 | .063 | .022 | .036 | .004 |
| 500 | .35 | .107 | .038 | .115 | .043 | .073 | .017 | .086 | .023 | .044 | .008 |
| 1000 | .175 | .121 | .014 | .121 | .006 | .079 | .006 | .088 | .002 | .045 | .001 |
| 2000 | .0875 | .135 | .014 | .131 | .010 | .086 | .007 | .097 | .009 | .047 | .002 |
| 3000 | .058 | .152 | .017 | .141 | .010 | | | | | .048 | .001 |
| 3500 | .050 | .166 | .014 | | | | | | | | |
| 4000 | .044 | .204 | .038 | .148 | .007 | .096 | .010 | .108 | .011 | .049 | .001 |
| 4500 | .039 | .266 | .062 | | | | | | | | |
| 5000 | .035 | .335 | .069 | .161 | .013 | .104 | .008 | .116 | .008 | .051 | .002 |
| 6000 | .029 | .439 | .104 | .174 | .013 | .137 | .033 | .138 | .022 | | |
| 8000 | .022 | .557 | .118 | .256 | .082 | .299 | .162 | .315 | .177 | | |
| 10000 | .0175 | .633 | .076 | .426 | .170 | .405 | .106 | .406 | .091 | .053 | .002 |
| 12000 | .0146 | .674 | .041 | .525 | .099 | .446 | .041 | .447 | .041 | | |
| 15000 | .0117 | .709 | .035 | .613 | .088 | .474 | .028 | .480 | .033 | .057 | .004 |
| 20000 | .00875 | .737 | .028 | .692 | .079 | .502 | .028 | .500 | .020 | .063 | .006 |
| 25000 | .0070 | .754 | .017 | .738 | .046 | .514 | .012 | .511 | .011 | .065 | .002 |
| 30000 | .0058 | .768 | .014 | .764 | .026 | | | | | .069 | .004 |
| 35000 | .0050 | | | .787 | .023 | .530 | .016 | .527 | .016 | .089 | .020 |
| 40000 | .0044 | .782 | .014 | .800 | .013 | | | | | .227 | .138 |
| 45000 | .0039 | | | | | .542 | .012 | .538 | .011 | .281 | .054 |
| 50000 | .0035 | .795 | .013 | .816 | .016 | | | | | .303 | .022 |
| 55000 | .0032 | | | .823 | .007 | | | | | | |
| 57000 | .0031 | | | | | | | | | .311 | .008 |
| 60000 | .0029 | .806 | .011 | | | .555 | .013 | .547 | .009 | | |
| 65000 | .0027 | | | .833 | .010 | | | | | .317 | .006 |
| 70000 | .0025 | .813 | .007 | | | | | | | | |
| 75000 | .00233 | | | | | | | | | .319 | .002 |
| 80000 | .0022 | .816 | .003 | .839 | .006 | .573 | .018 | .552 | .005 | | |
| 85000 | .00206 | | | | | | | | | .319 | .000 |
| 90000 | .00194 | .820 | .004 | | | | | | | | |
| 100000 | .00175 | .847 | .027 | .846 | .007 | .580 | .007 | .571 | .019 | .319 | .000 |

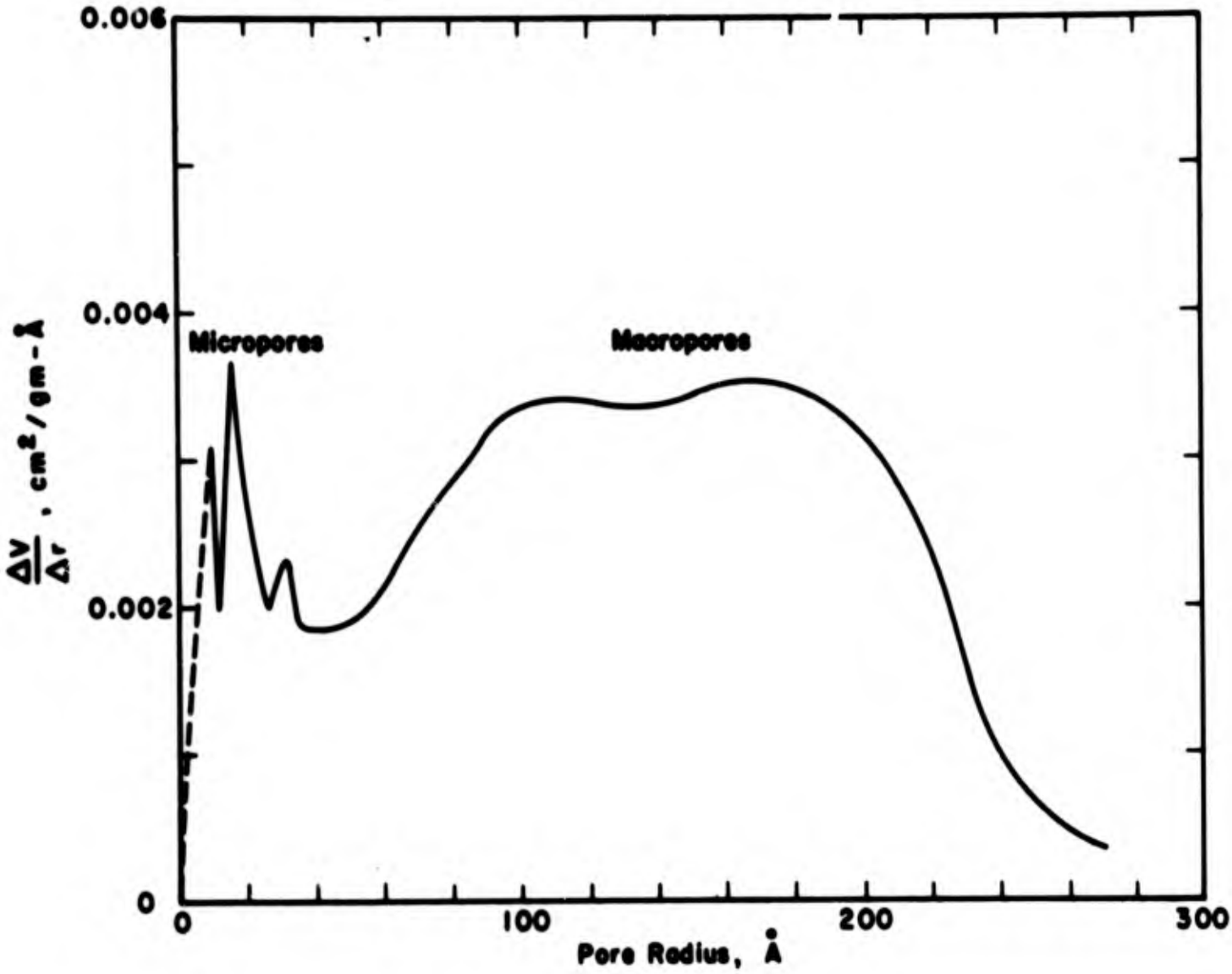


Figure 3. Pore Size Distribution Data For Apachi 1049-100

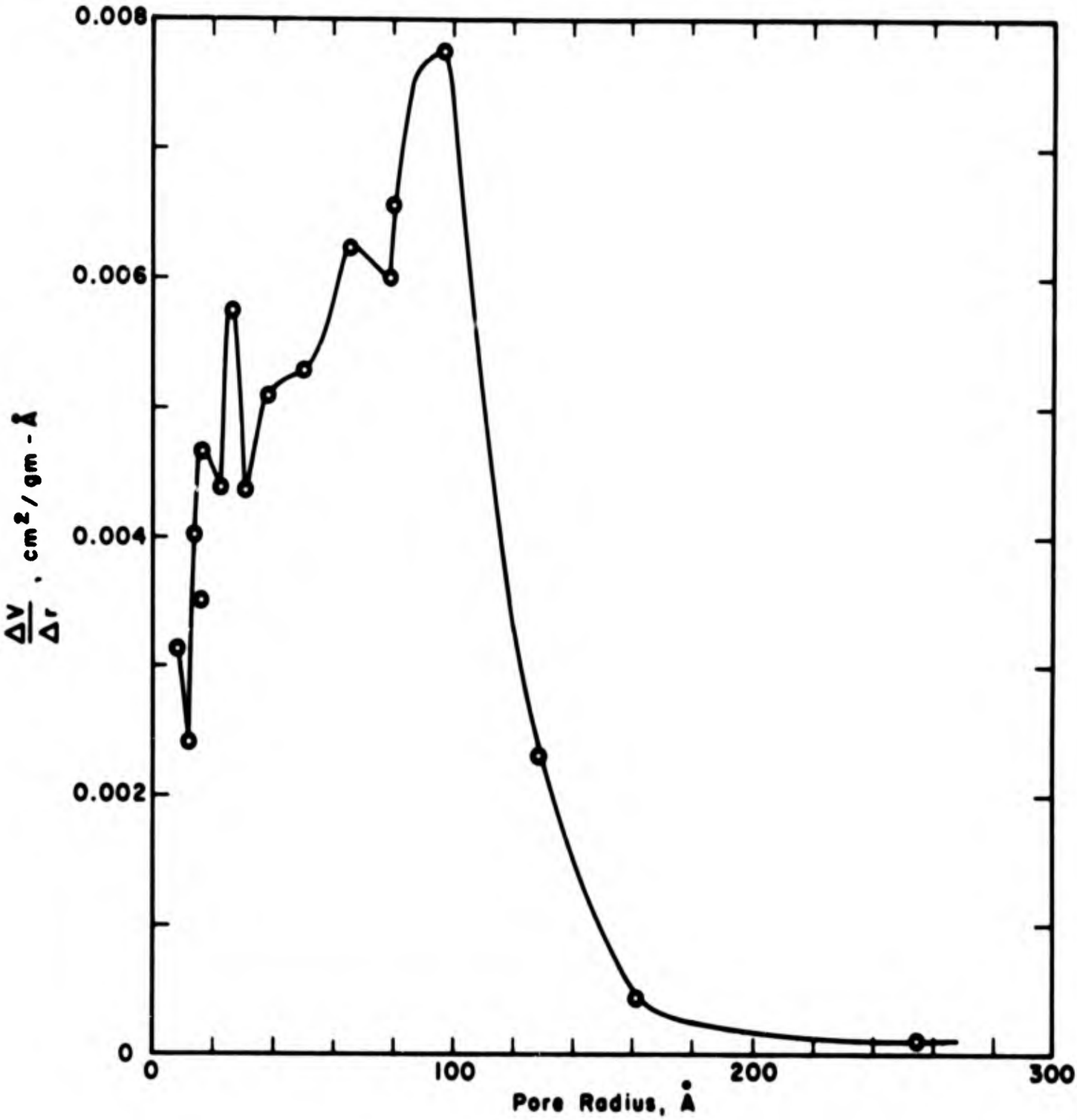


Figure 4. Pore Size Distribution Data For Apachi 1070-82

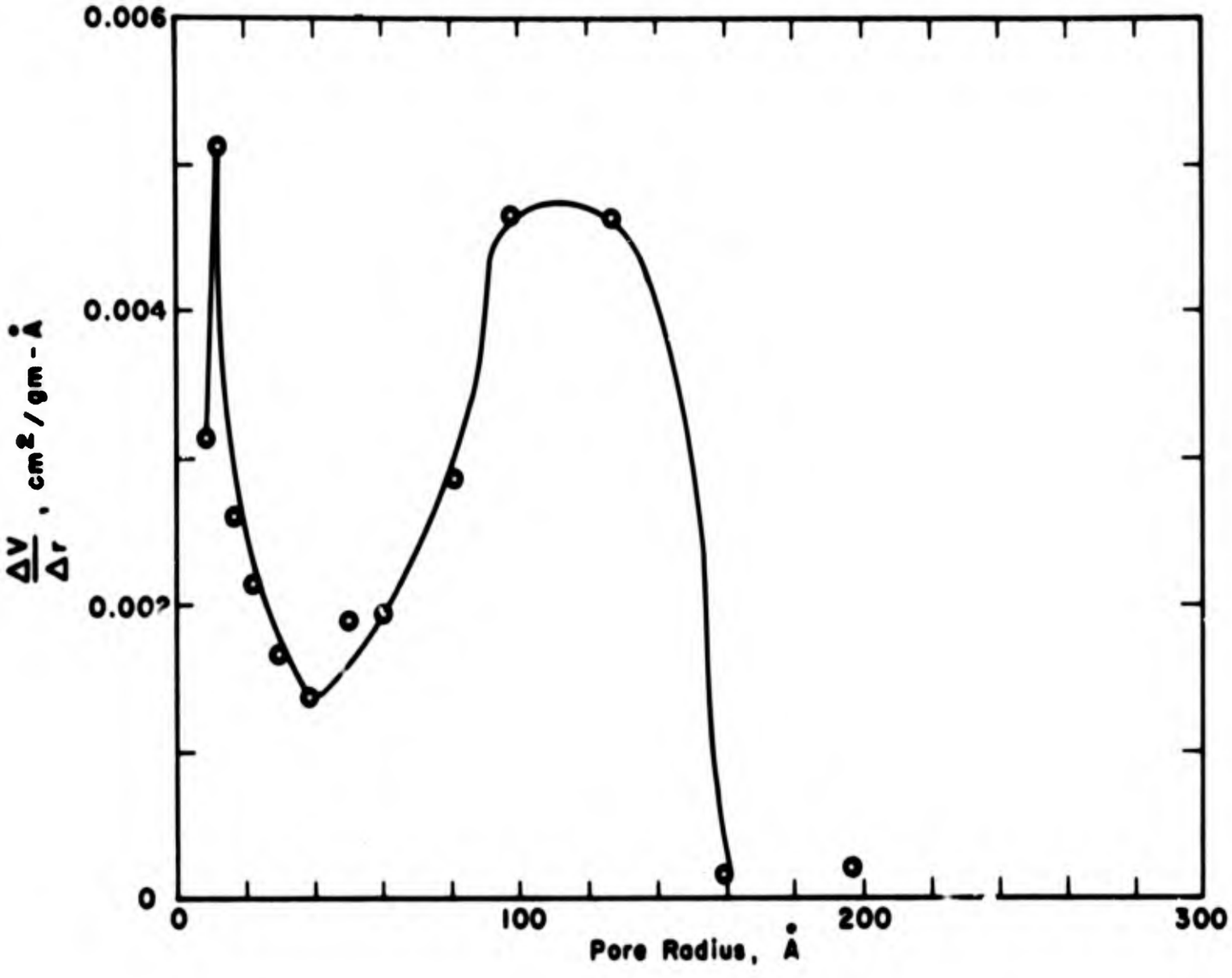


Figure 5. Pore Size Distribution Data For Apachi 1070-95

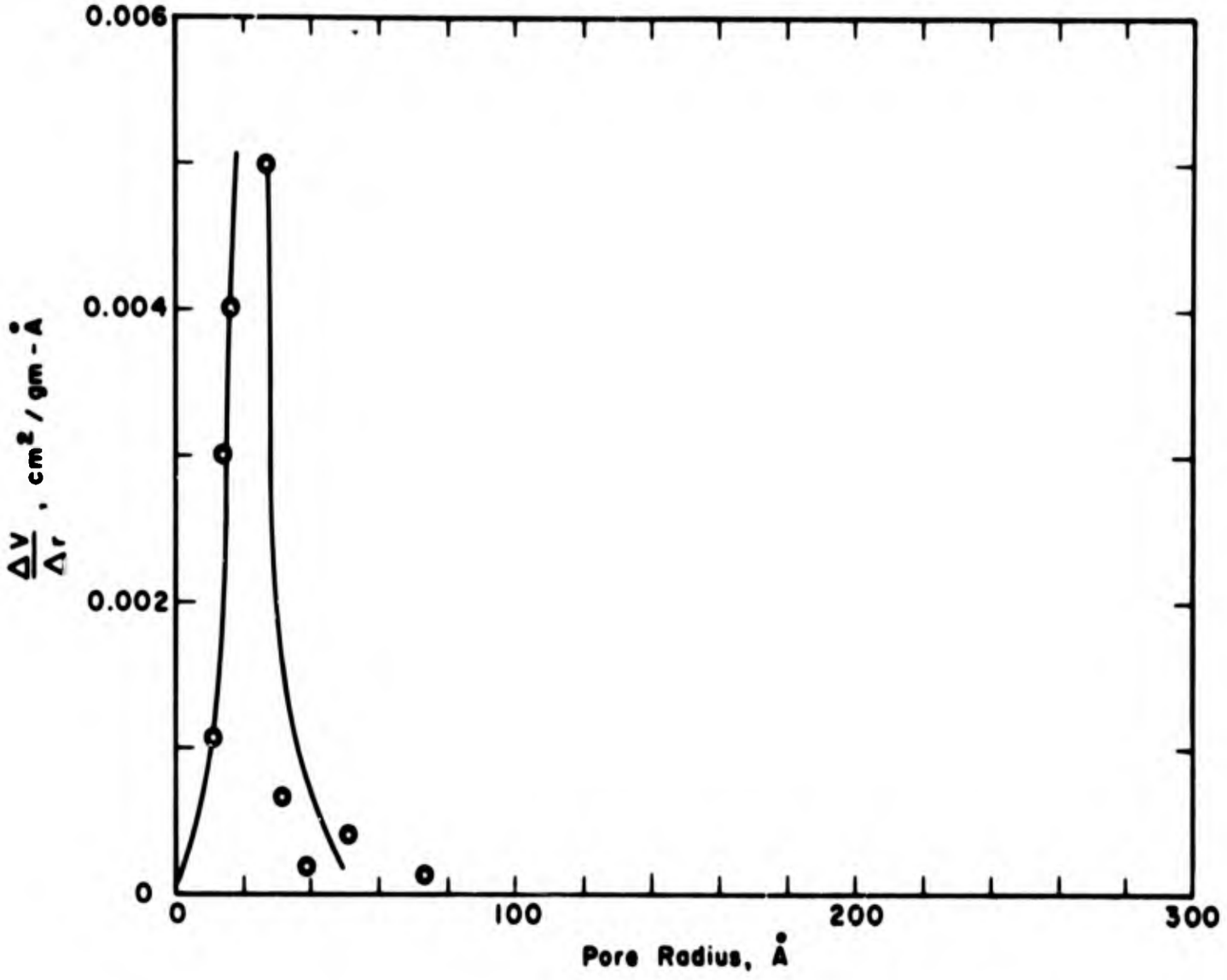


Figure 6. Pore Size Distribution Data For Cryenco Ferric Oxide Gel

$$V_m = \pi \bar{r}^2 \bar{L} \quad (14)$$

$$A = 2\pi \bar{r} \bar{L} \quad (15)$$

where

$V_m$ = micropore volume, $cm^3/gm$

A = surface area, $cm^2/gm$

n = number of pores per gram

$\pi$ = 3.14

$\bar{r}$ = average micropore radius, cm

$\bar{L}$ = average micropore length, cm

Dividing Equation 14 and 15 leads to an expression for the average micropore radius in terms of the micropore volume and surface area:

$$\bar{r} = 2\,V/A \quad (16)$$

The results obtained using Equation 14 agree very well with the average values obtained from Figures 3 through 6.

| Catalyst | Average Micropore Radius | |
|---|---|---|
| | Calculated | Graphical |
| 1049-100 | 18.2°A | 16 |
| 1070-95 | 16.7 | 16 |
| Ferric Oxide Gel | 22.3 | 22 |

2. Adsorption of Hydrogen on APACHI Catalysts.

Date on the adsorptive capacity of APACHI 1049-100 was obtained on another program (2). This date is reproduced in Figure 7.

3. Effect of Flow Rate

All of the Air Products' ortho-parahydrogen catalyst activity determinations were conducted with hydrogen

BLANK PAGE

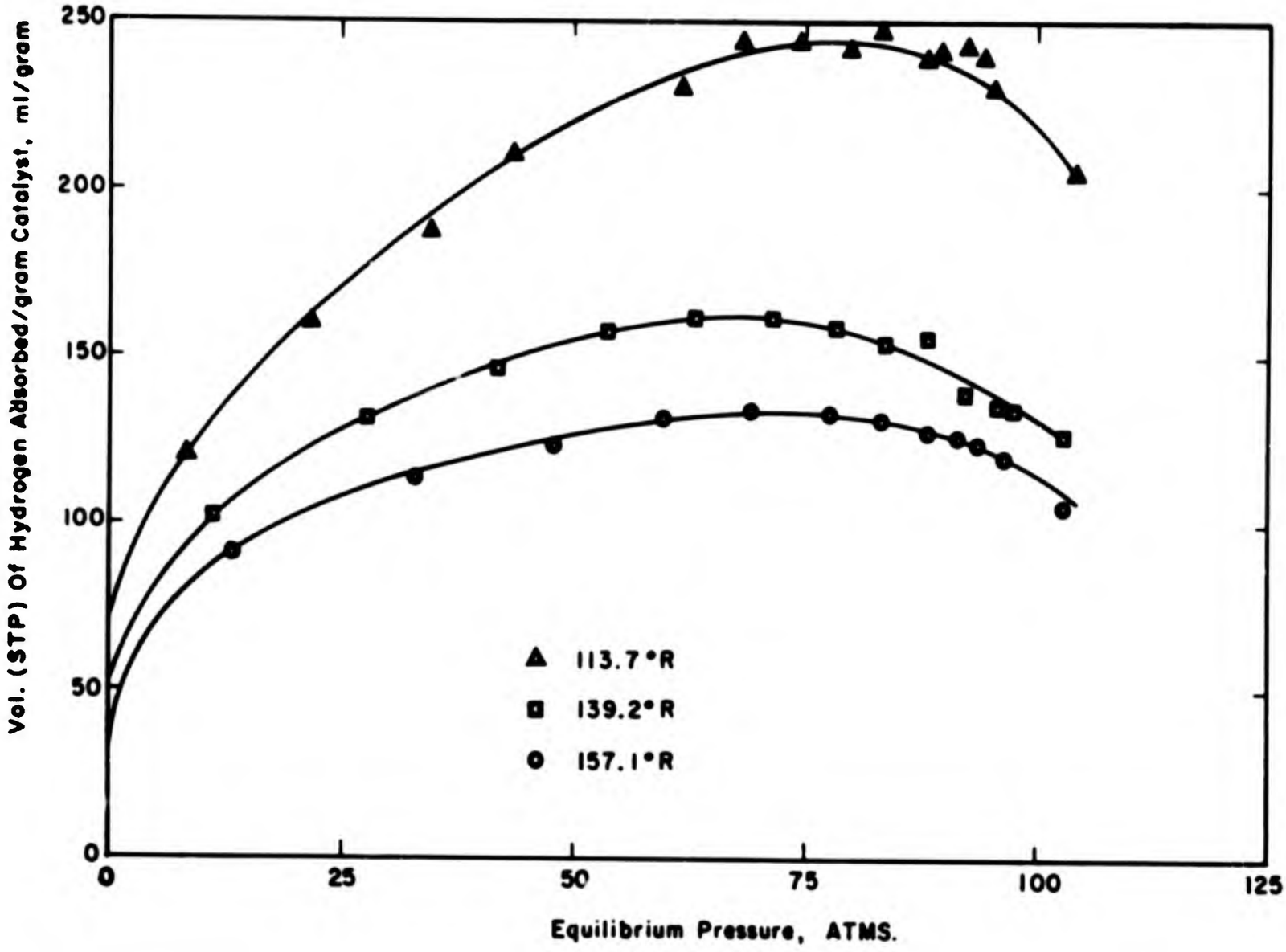


Figure 7. Adsorption Isotherms Of Hydrogen On Apachi 1049-100

flow rate as a parameter. Consequently, no additional experimentation in this area was needed; instead, the prior results were reviewed and reinterpreted in light of the theoretical studies of rate limitation.

For the constant catalyst mass ortho-parahydrogen reactor utilized by Air Products, an increase in flow rate is equivalent to an increase in the concentration log mean driving force. A typical graph, Figure 8, of experimental reaction rate versus log mean driving force is presented here; other examples can be found elsewhere in this report.

4. Effect of Pressure

The effect of pressure was determined by measuring reaction rate as a function of log mean driving force, with pressure as a parameter. At a temperature of -320°F, the pressure range studied was from 50 to 1500 psig; two catalysts, APACHI 1049-100 and 1130-22 were utilized; and the catalyst particle size was varied from 20 to 100 mesh (840 to 149 microns). In this manner, most of the critical variables were studied parametrically with pressure, Figures 9 through 13 illustrate the results for the 1049-100 catalyst; Figure 14 combines these results on one graph for comparison.

5. Effect of Catalyst Particle Size

In order to determine the effect of catalyst particle size, reaction rate was determined as a function of the concentration log mean driving force, with particle size as a parameter. Two APACHI catalysts, 1049-100 and 1130-22, were studied. The results were very similar and consequently only the data for 1130-22 will be presented here. The particle size was varied from 20-25 to 80-100 mesh (arithmetic average catalyst diameters of 775 to 163 microns). Figure 15 is a graphical presentation of these results.

6. Analysis of Experimental Error

Before any experiments were made for the purpose of rate limitation analysis, a statistical analysis of experimental error was performed to determine the maximum possible experimental deviation. This is defined as the summation of the known experimental inaccuracies. When a change

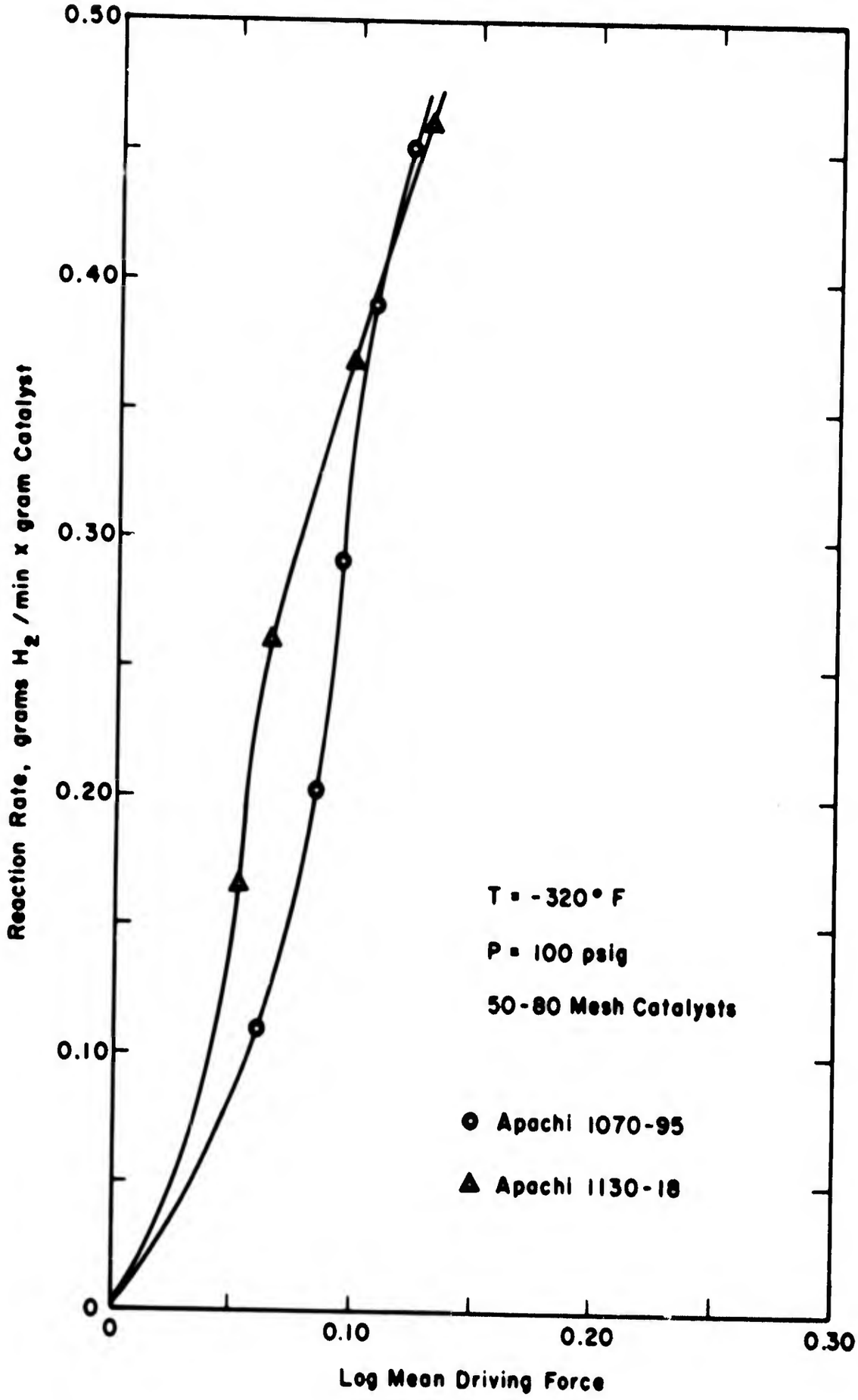


Figure 8. Experimental Conversion Rate Versus Log Mean Driving Force

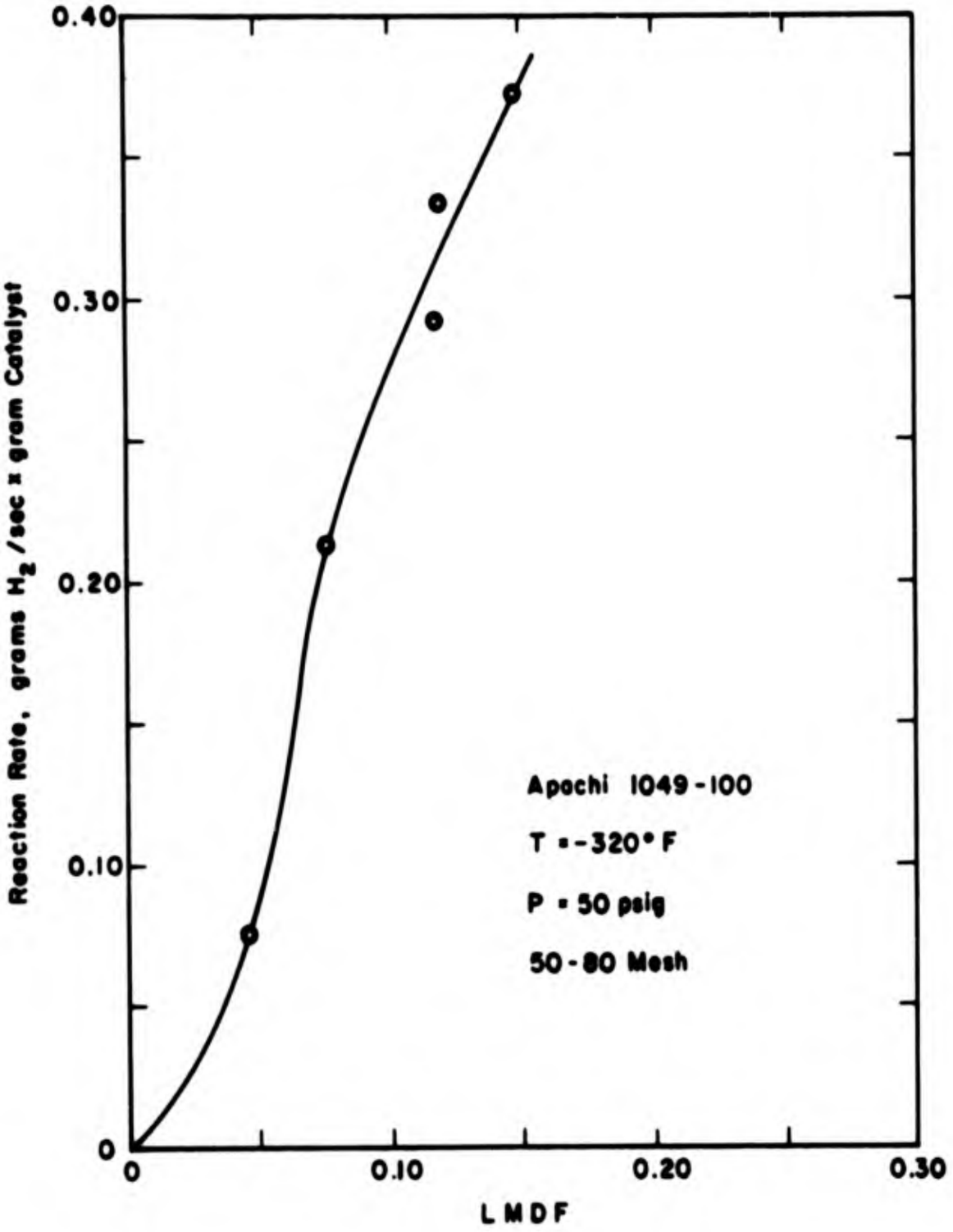


Figure 9. Reaction Rate Versus Log Mean Driving Force

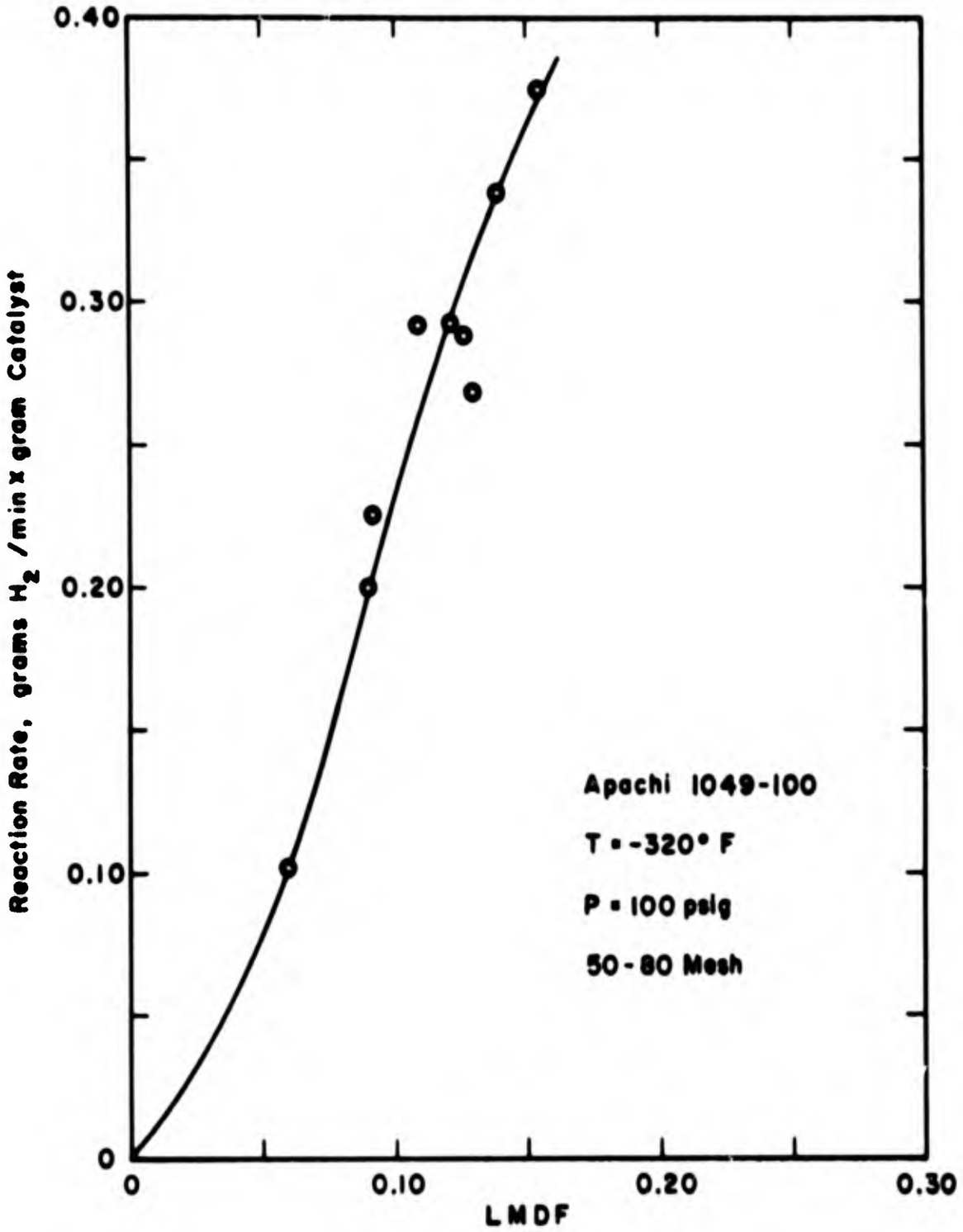


Figure 10. Reaction Rate Versus Log Mean Driving Force

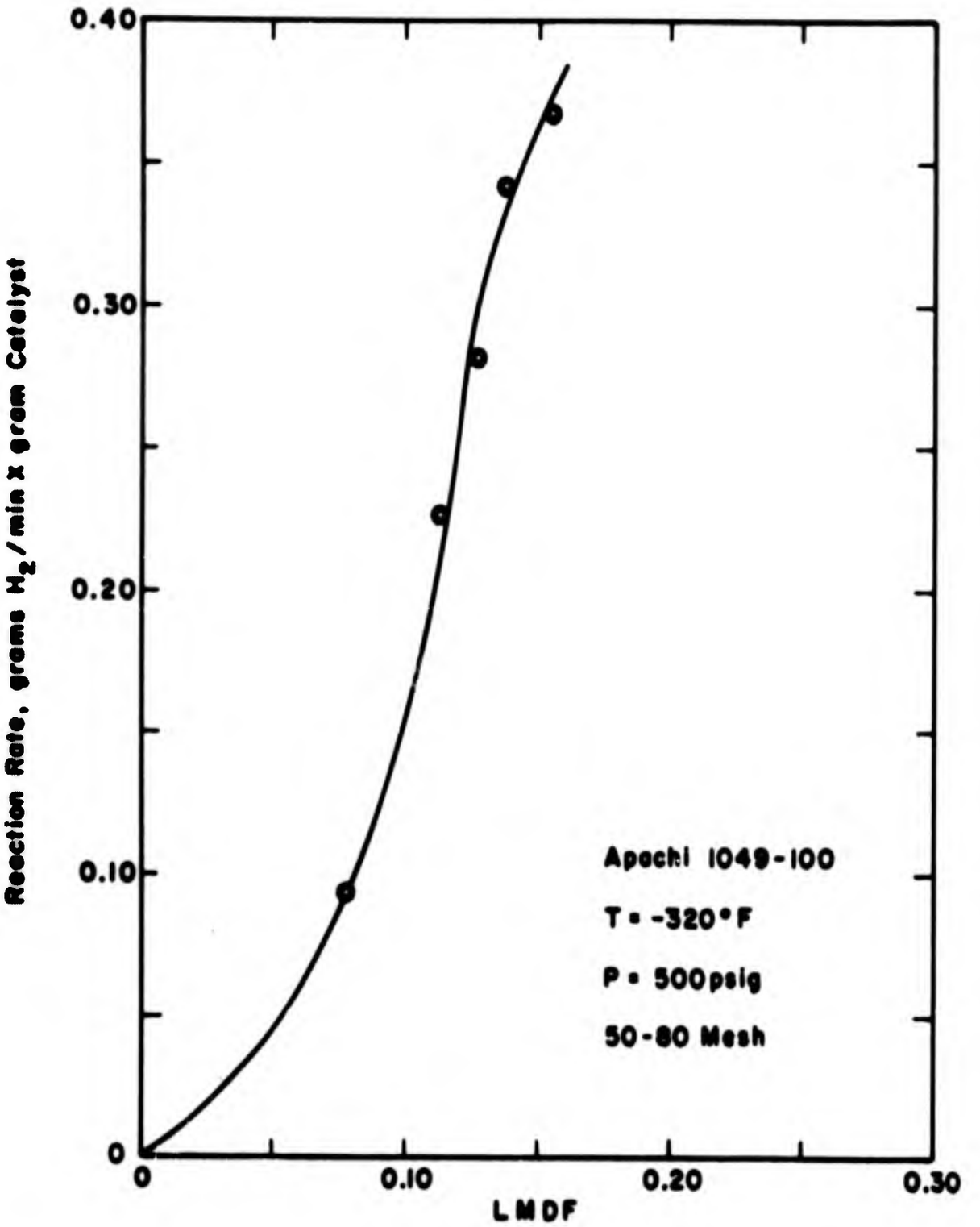


Figure 11. Reaction Rate Versus Log Mean Driving Force

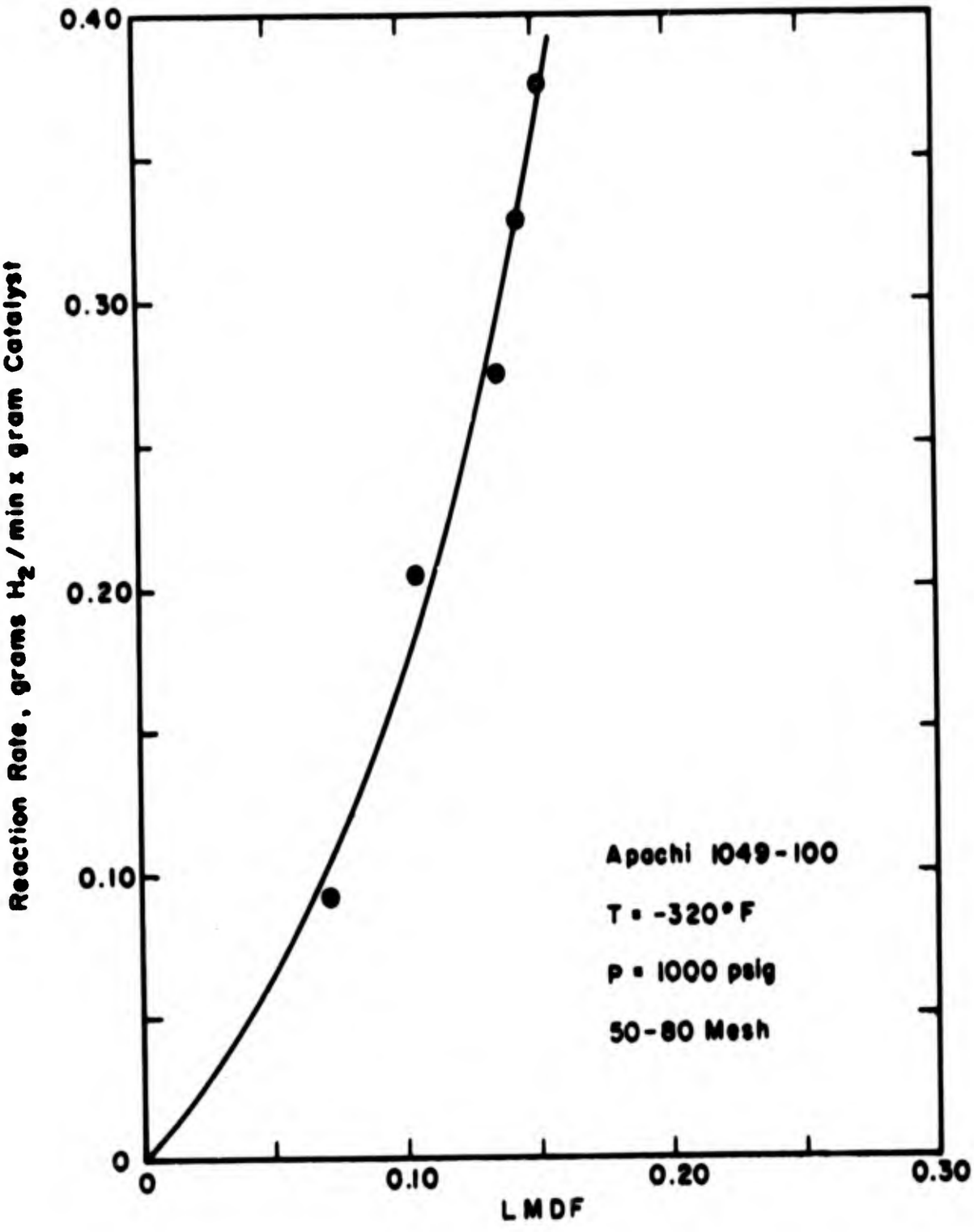


Figure 12. Reaction Rate Versus Log Mean Driving Force

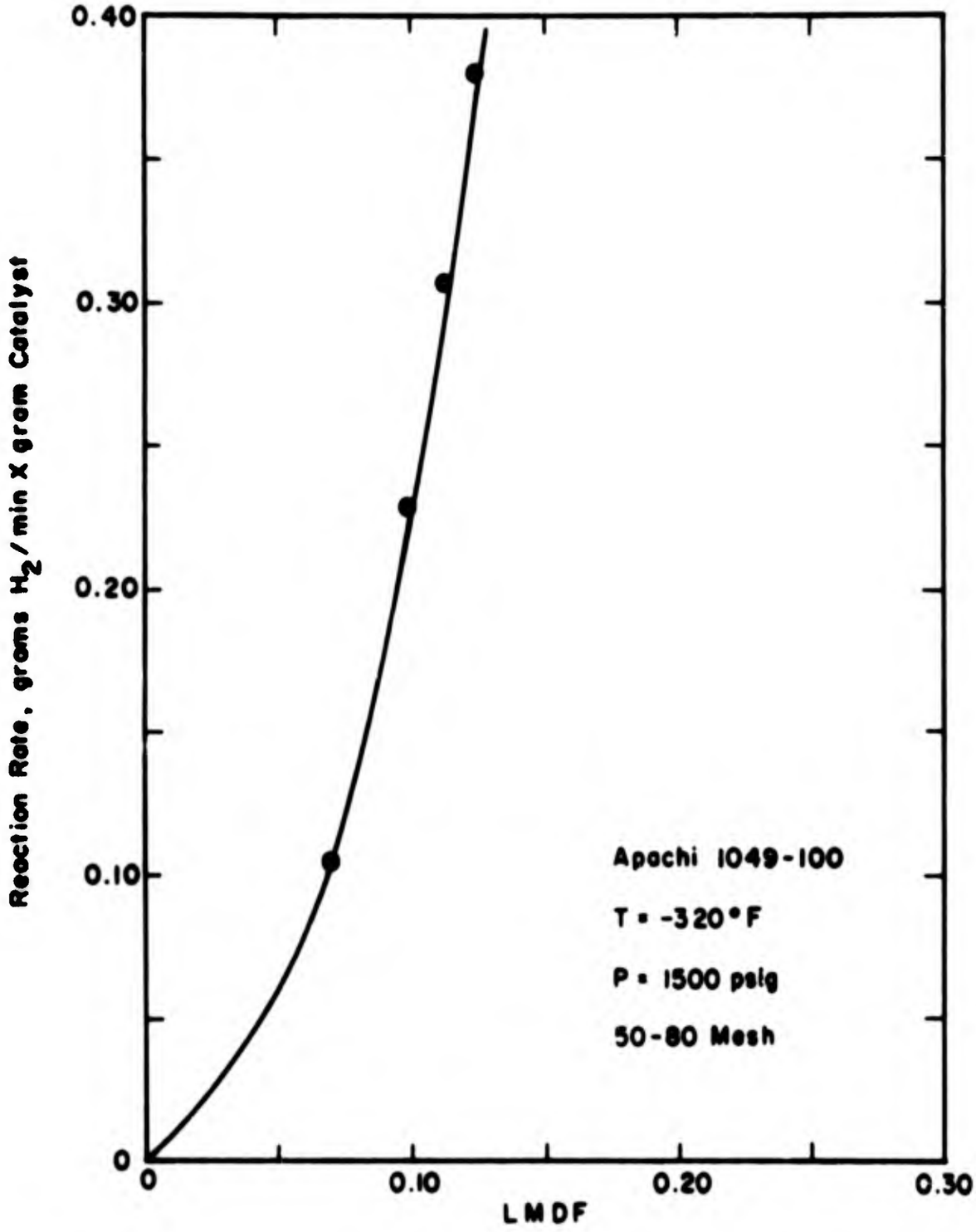


Figure 13. Reaction Rate Versus Log Mean Driving Force

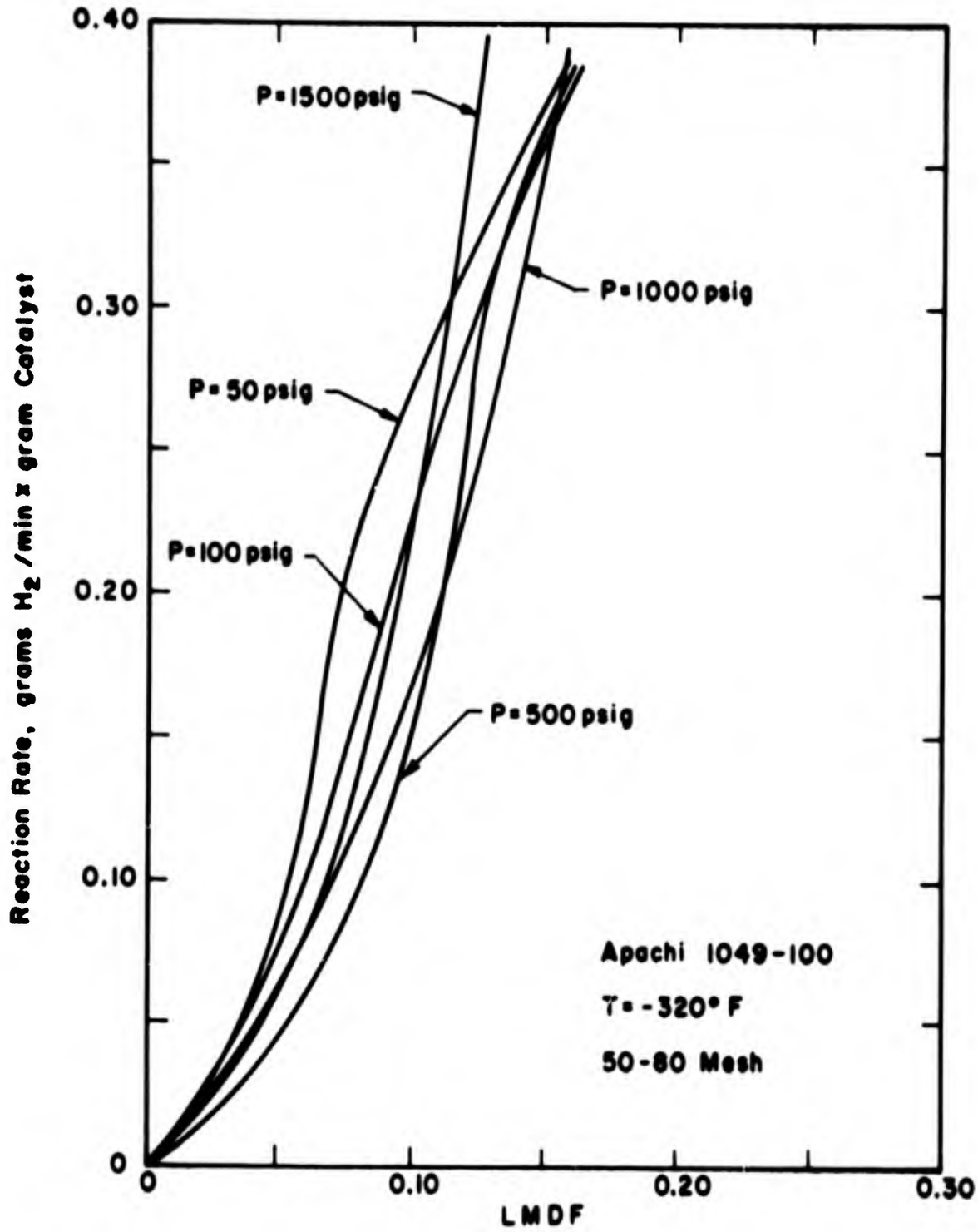


Figure 14. Reaction Rate Versus Log Mean Driving Force With Pressure As Parameter

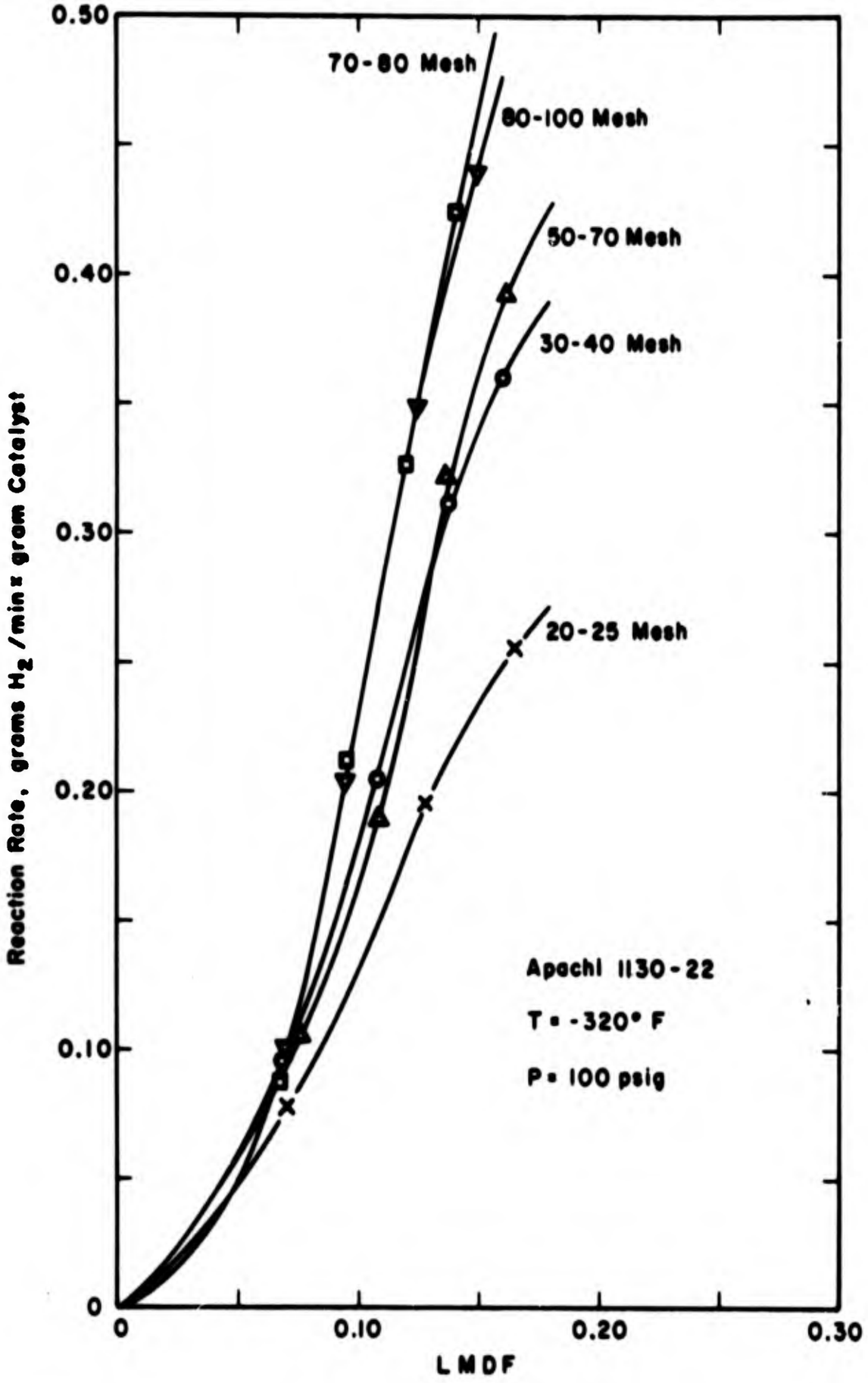


Figure 15. Experimental Conversion Rate Versus Log Mean Driving Force With Particle Size As A Parameter

in a variable is made, its effect cannot be considered significant unless it is larger than the maximum possible experimental deviation.

The maximum possible experimental deviation is calculated by estimating the individual errors associated with the various experimental measurements, such as pressure, temperature, etc. These errors are then combined, with the aid of the kinetic rate equation for the reactor, in a manner which would maximize the resultant -- the expected reaction rate deviation. In essence, the maximum possible experimental deviation is that value which would be experienced when all of the possible individual errors occurred at the same time.

The statistical analysis was performed under the assumption that the catalyst particle size was maintained as a constant, and the results predicted that the maximum expected experimental deviation in reaction rate should be no larger than 5%, at a LMDF of 0.13. But, a series of reproducibility runs performed in conjunction with the analysis of error resulted in unexplainable deviations as large as 20% -- much higher than the anticipated value.

At the time of the error analysis, all APCI ortho-para-hydrogen conversion studies were performed with a 50 to 80 mesh catalyst size range. It can be seen from Figure 15 that the difference in reaction rate between 50 to 70 and 70-80 mesh catalyst particles, at an LMDF of 0.13, is 23%. Consequently, the unexplained deviations experienced earlier were probably due to the fact that the 50 to 80 mesh catalyst samples were not homogenous with respect to particle size.

This experimental discrepancy has now been eliminated. The standard catalyst activity determinations are now performed with rigidly-controlled 70 to 80 mesh catalyst samples, and the experimental errors have been reduced to less than 5%.

## C. INTERPRETATION OF THE THEORETICAL ANALYSES ON THE BASIS OF THE EXPERIMENTAL RESULTS

In the previous sections, theoretical analyses of each of the possible ortho-parahydrogen conversion steps were discussed,

the expected effect of prime experimental variables were postulated on the bases of the theories, and the results of planned experimental verification were presented. Each of the theoretical analyses will now be interpreted in light of the experimental data and the conclusion will be a definition of the conversion limitation. These results in turn will allow a scientific optimization of ortho-parahydrogen catalysts.

1. Bulk Diffusion

The theoretical analysis of the bulk diffusion limitation predicted that the effect of flow rate and therefore log mean driving force would be as depicted in Figure 1. It can be seen, in Figures 8 through 13, that the experimental relationship between the reaction rate and LMDF follows this pattern only at high pressures and small catalyst particle diameter.

A 4% increase in reaction rate for a 1220% increase in pressure was postulated, and for the same conditions, a 23% increase was experimentally measured.

An increase in reaction rate by a factor of 8 was predicted, and an increase of a factor of 1.9 was measured when the catalyst particle size was decreased from 20-25 to 80-100 mesh.

Although no pore size distribution effect should be observed if bulk mass transfer was the limitation, an effect was measured.

In conclusion, it can be said the bulk diffusion alone does not limit the process but it is of influence.

2. Pore Diffusion

The measured relationship between reaction rate and LMDF does not follow the effect predicted for a pore diffusion controlled system. The same can be said for the pressure effect. But the importance of pore diffusion becomes apparent when the results of the pore size distribution and catalyst particle size experimentation are analyzed.

For pore diffusion limitation, the theoretical analyses resulted in Equation 5, as follows:

$$R_r = k_f E_p (LMDF).$$

In addition, the analyses indicated that the pore diffusion effectiveness factor is a function of catalyst particle diameter. The experimental results, Section II - B - 5 did indeed show a particle size effect. In terms of effectiveness factors, these experimental results for APACHI 1049-100 and 1130-22 are graphically compared to the values obtained from theory in Figures 16 through 18. Figure 19 shows the method of evaluating $k_f$.

3. Bulk Diffusion, Pore Diffusion, and Surface Reaction Combined Limitation

The graphs of reaction rate versus LMDF presented in this report contain many examples of the "S" shaped curve predicted by the theoretical analysis of combined resistances and illustrated in Figure 2.

The experimental results show that the effect of pressure appears to be a hybrid of the postulated effects when bulk and pore diffusion individually limit the process. Theoretically, it was shown that bulk diffusion is only a weak function of pressure, while both pore diffusion and surface reaction are approximately directly proportional to pressure. Thus, as pressure is increased, the resistance due to pore diffusion and surface reaction should decrease, while the resistance due to bulk diffusion should remain essentially constant. This behavior was observed experimentally in the data of Figure 14, which shows a gradual shift from the "S" shaped log mean driving force curve at low pressure to the charateristically shaped curve for bulk diffusion controlled conversion rate at high pressure.

The effects of the other variables studied - catalyst pore size distribution and particle size - fall into the same category, in between that predicted by the bulk and pore diffusion analyses.

It was concluded, therefore, that the conversion rate was limited by a combination of the bulk diffusion, pore diffusion, and surface reaction resistances. Thus the observed reaction rate can be expressed as follows:

$$\text{Observed Reaction Rate} = \frac{F}{W}(y_1 - y_2) = k_f E_B E_P (LMDF).$$

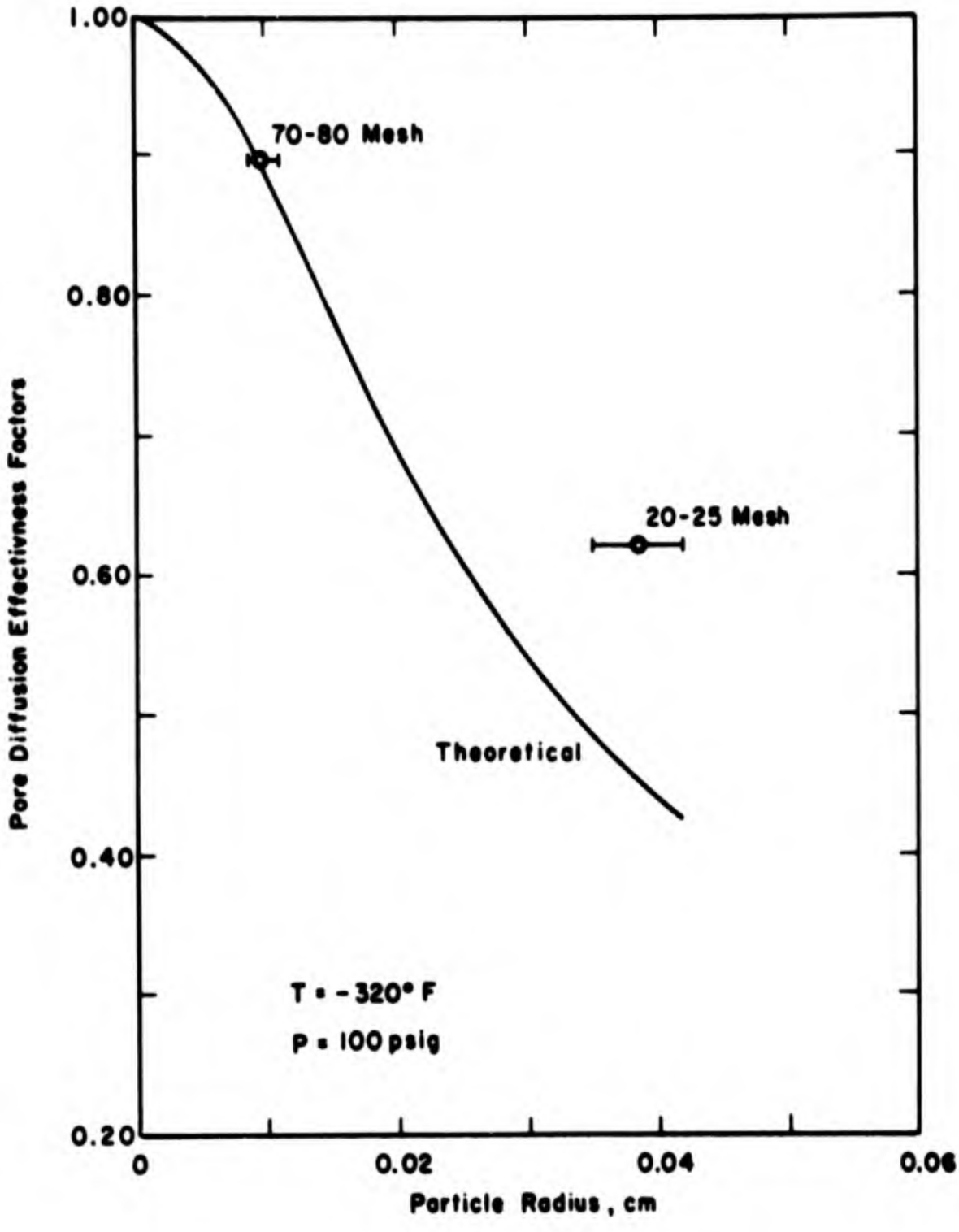


Figure 16. Pore Diffusion Effectivness Factor For Apachi 1049-100

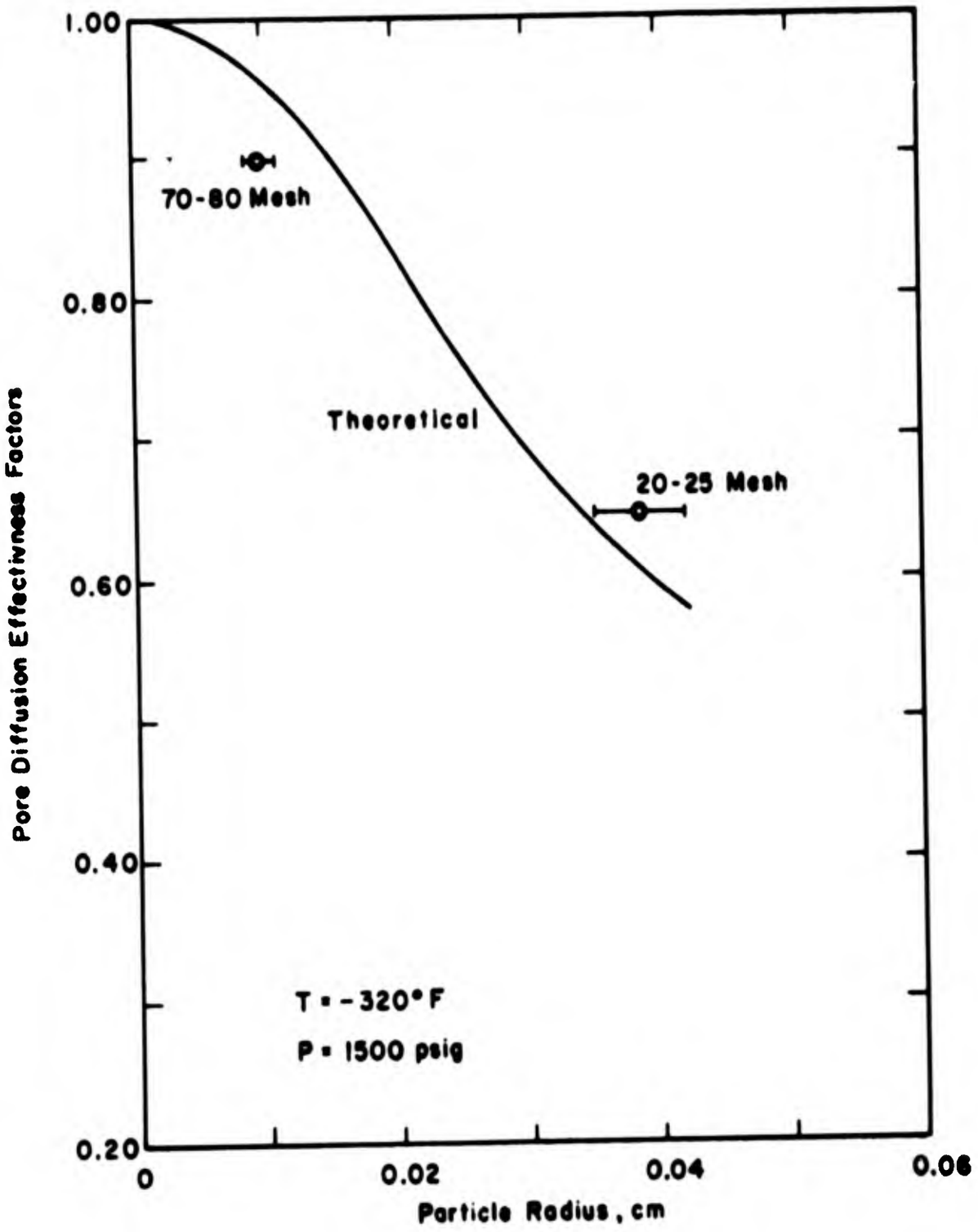


Figure 17. Pore Diffusion Effectivness Factor For Apachi 1049-100

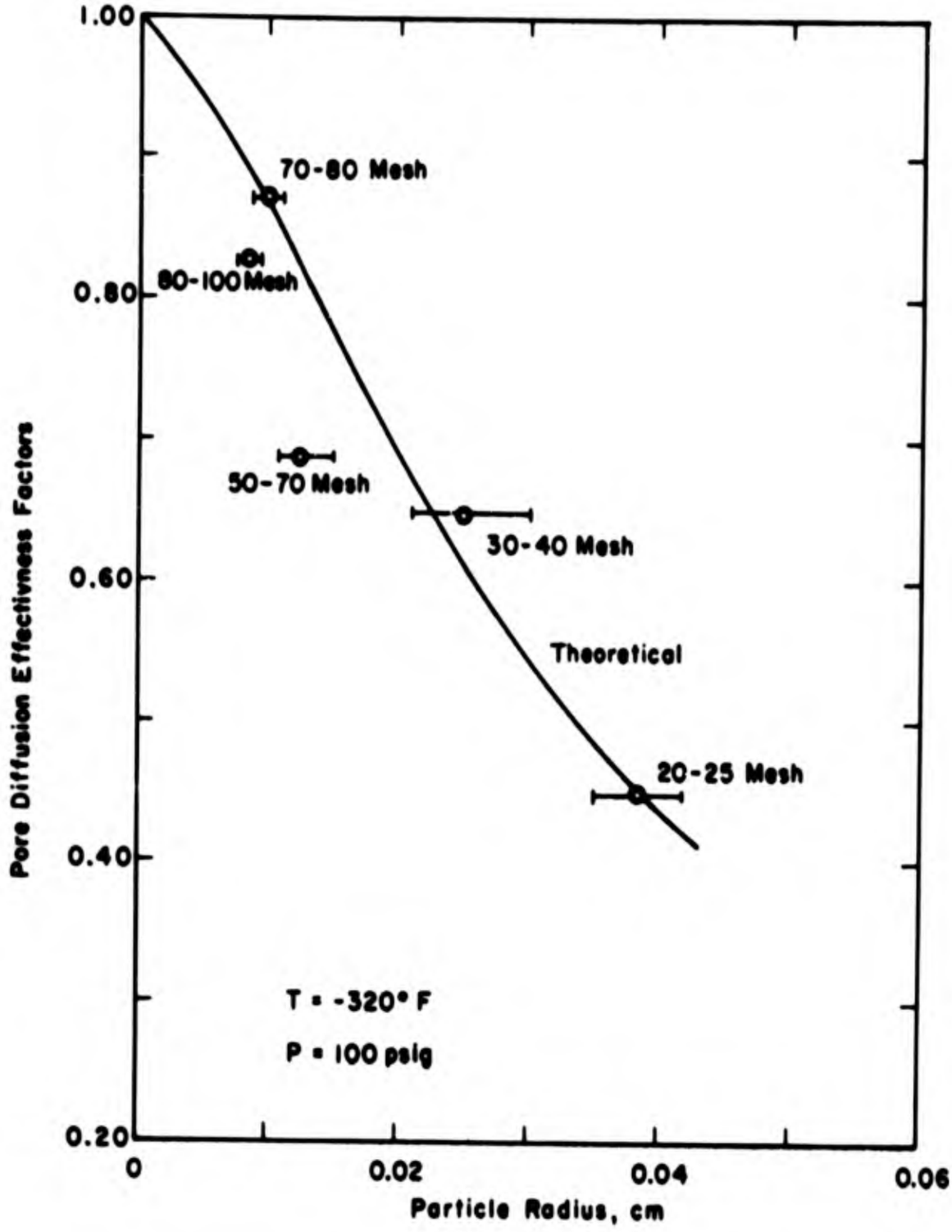


Figure 18. Effectivness Factor Versus Particle Radius For Apachi 1130 - 22

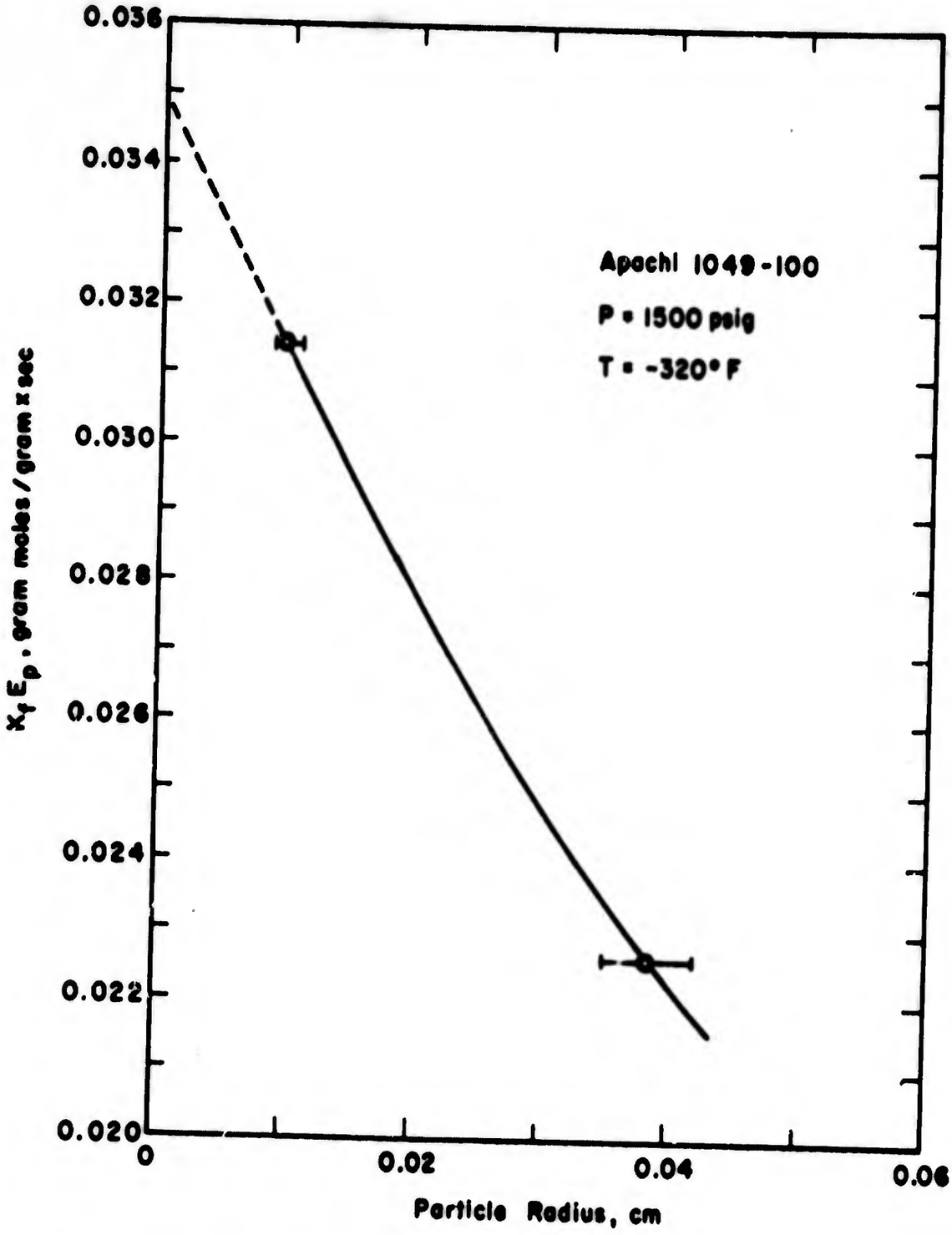


Figure 19. Experimental Data For The Calculation Of Pore Effectiveness Factor

# III. EFFECT OF ADSORBED NITROGEN ON CATALYTIC ACTIVITY

## A. SCOPE

An experimental program was undertaken to measure the effect of adsorbed nitrogen upon the catalytic activity of ortho-parahydrogen conversion catalysts. The test program provided eight pairs of data points for a combination of three different catalysts, three temperatures, and two different nitrogen-in-hydrogen contaminant levels. Each pair of data points provides a catalytic activity before and after nitrogen adsorption (4).

## B. EXPERIMENTAL APPARATUS

The experimental apparatus used for the set of experiments described in this report was in the main as described by Schmauch et al (3). A simplified flow sheet is presented in Figure 20. Hydrogen, or hydrogen containing low concentrations of nitrogen, was contained in cylinders and was fed from them with regulated flow and pressure to the catalyst test chamber. The catalyst bed temperature control at the three temperatures used was obtained by: a) normal boiling point of oxygen, -297°F; b) normal boiling point of nitrogen, -320°F; c) triple point of nitrogen, -346°F. Hydrogen containing zero impurities was obtained by passing the gas through a Deoxo unit, a drier, colling coils, and silica gel adsorbers at liquid nitrogen temperature. This purified gas was then passed through the test catalyst bed, the parahydrogen content being determined at the inlet and outlet by thermal conductivity. Hydrogen containing a standard quantity of nitrogen impurity, 60 or 680 ppm, was passed through cooling coils directly to the test catalyst chamber, having previously been purified. The nitrogen content was continuously monitored and recorded by a thermal conductivity apparatus, with the cell operating at room temperature. A sensitivity of $\pm$ 5 ppm was achieved with a span of 60 ppm and about $\pm$ 10 ppm with a span of 680 ppm of nitrogen. The hydrogen stream to be analyzed for its nitrogen content was always passed through an ambient temperature normalizing catalyst bed just before entry to the thermal conductivity cell. This was necessary to eliminate the effect of varying ratios of ortho to parahydrogen upon the thermal conductivity analysis. The ortho to para ratio was determined by thermal conductivity analysis, a different analyzer being used. Since nitrogen was present in some of the streams to

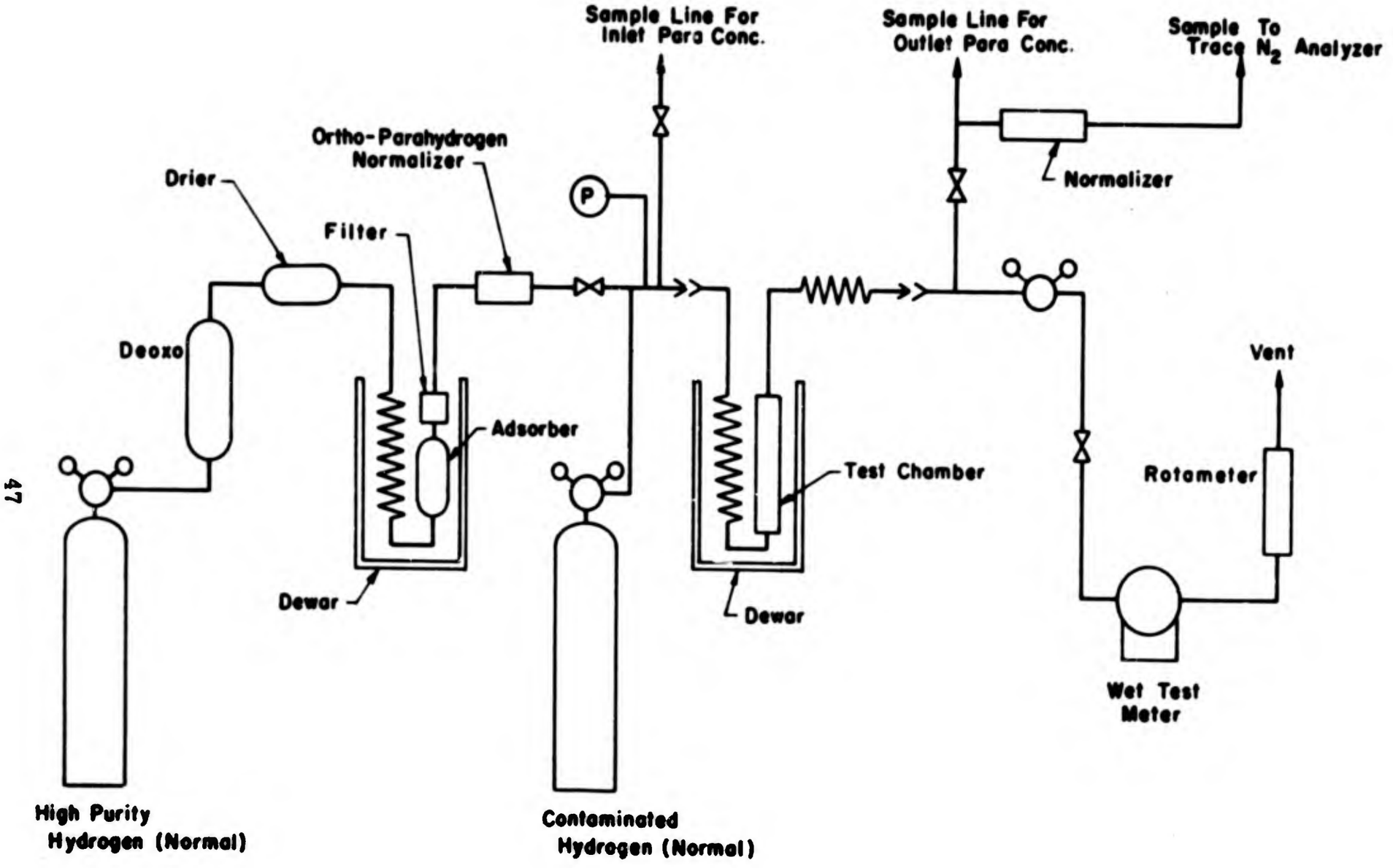


Figure 20. Ortho-Parahydrogen Test Apparatus Flowsheet

be analyzed for the ortho to parahydrogen ratio, it was necessary to add the nitrogen content contribution from the thermal conductivity reading. This could be done straightforwardly after suitable calibration of the ortho-parahydrogen analyzer with hydrogen of known ortho-parahydrogen content and known ppm concentrations of nitrogen. The usual procedure was to zero the analyzer with pure normal hydrogen, span with pure hydrogen of a known higher parahydrogen concentration, and calibrate with normal hydrogen containing a known concentration of nitrogen contaminant. The indicated parahydrogen concentration is reduced below the true value in proportion to the amount of nitrogen which is present as an impurity.

## C. EXPERIMENTAL PROCEDURES

Run No. 3 will be described in some detail to illustrate the experimental method.

A cylinder with hydrogen containing 680 ppm of nitrogen and essentially no other impurities (dew point below -100°F; oxygen less than 1 ppm; etc.) was connected to the manifold along with pure hydrogen for system purging. The catalyst to be tested, contained in a small catalyst bed in which it had been previously reactivated in a flowing nitrogen stream at 150°C for two hours, was placed in the flow circuit. The 0.25-in. I. D. x 6.0-in. long bed contained 1.7134 gms of 30-50 mesh catalyst. Nitrogen was purged from the system by a flow of pure hydrogen; the hydrogen flow was continued as liquid nitrogen was added to the bath surrounding the catalyst bed. Hydrogen flow was established at approximately 0.1 SCFM as measured by means of a wet test meter at the flow system exit; the pressure was regulated to 100 psig; the thermal conductivity analyzers for the ortho to parahydrogen ratio and for nitrogen were zeroed and spanned.

With all the experimental apparatus working in acceptable fashion, the response of the catalyst bed was further checked by measuring the steady state inlet and outlet parahydrogen concentrations at several flow rates, starting with the 0.1 SCFM rate already established. Data for these several flows are listed in Table 3 and plotted in Figures 21 and 22, Curves (A). After the preliminary runs with pure hydrogen had been completed, the flow rate was reset to 0.1 SCFM and the gas feed to the system was switched from pure hydrogen to the hydrogen containing 680 ppm of $N_2$. Holding flow rate, temperature, and pressure constant, the run was continued while recording the effluent parahydrogen concentration and effluent

BLANK PAGE

## TABLE 3

## VARIATION IN ORTHO-PARAHYDROGEN CONVERSION WITH FLOW RATE

| $H_2$ Flow SCFM | Inlet concn. % p-$H_2$ | Outlet concn. % p-$H_2$ | Gms $H_2$/min / gm. cat. | Gms $H_2$ conv./min / gm. cat. | $\frac{C_i - C_o}{\ln \frac{C_i - C_e}{C_o - C_e}}$ |
|---|---|---|---|---|---|
| 0.091 | 26.3 | 50.7 | 0.124 | 0.030 | 0 |
| 0.171 | 25.8 | 50.3 | 0.233 | 0.057 | 0.059 |
| 0.240 | 25.4 | 49.9 | 0.328 | 0.080 | 0.071 |
| 0.298 | 25.2 | 49.3 | 0.407 | 0.098 | 0.083 |

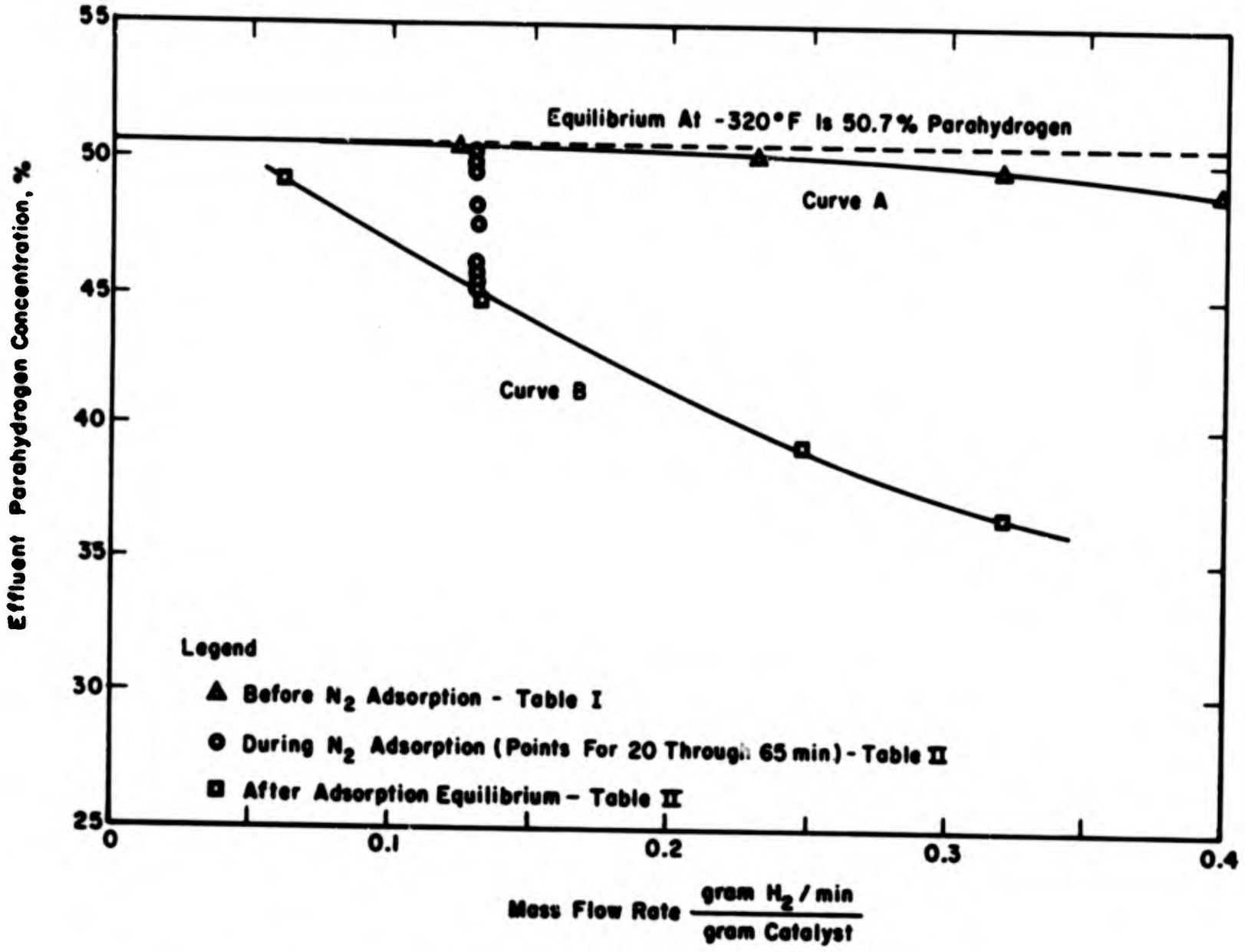


Figure 21. Ortho-Parahydrogen Conversion As A Function Of Flow Rate
Run No. 3

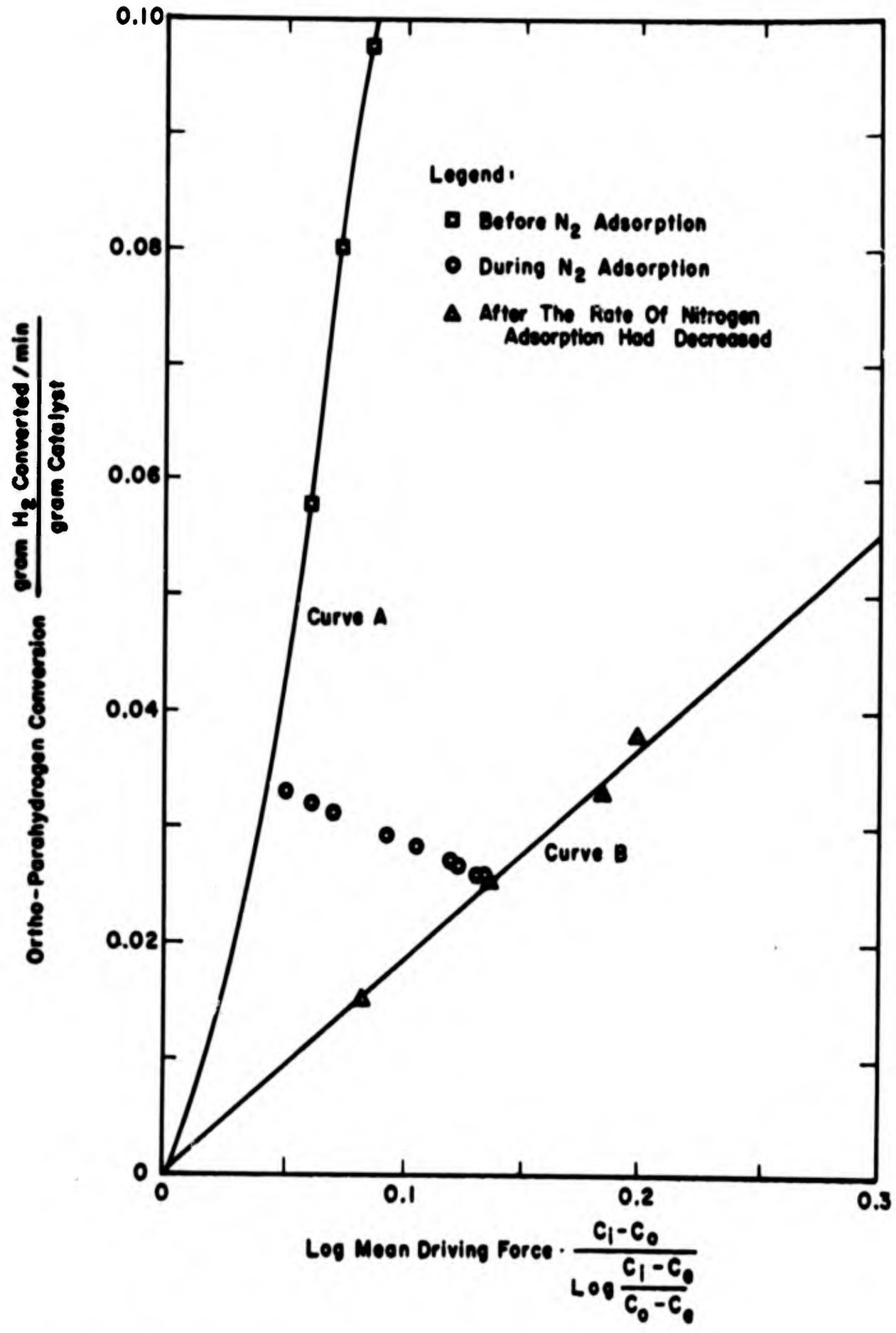


Figure . Ortho-Parahydrogen Conversion As A Function Of Log Mean Driving Force - Run No. 3

nitrogen concentration. The run was continued until the effluent concentration of nitrogen was the same as the inlet, at which time the parahydrogen concentration was noted to be constant. The flow rate was again varied to determine the outlet parahydrogen concentration as a function of flow in the same fashion as had been done at the beginning of the run. Data from the chart records are presented in Table 4 and plotted in Figures 21, 22 and 23.

## D. EXPERIMENTAL RESULTS

Continuing with Run No. 3, it may be noted from Figure 21 that as the flow rate of hydrogen is increased the effluent parahydrogen concentration decreases. If the rate of conversion is plotted as a function of the logarithmetic mean driving force, calculated in Table 4 and plotted in Figure 22, Curve (A), it is seen that a curve with the slight "S" shape results. This indicates that for the conditions of the experiment, the combined resistance of bulk diffusion, pore diffusion, and surface reaction is controlling the rate.

Figure 23 pictorially shows how the catalyst bed changes in performance as nitrogen is adsorbed. The initial parahydrogen concentration in the reactor effluent at zero time is seen to be the same as was obtained with pure hydrogen at a 0.10 SCFM flow rate, which is as expected, since essentially no nitrogen has yet entered the catalyst bed. As the flow continues it is noted that the effluent hydrogen contains a steadily decreasing content of parahydrogen and no nitrogen. The entering nitrogen, 680 ppm, is being entirely adsorbed. After a total of about 5.2 cubic feet of hydrogen, a few ppm of nitrogen appear in the effluent stream and shortly the concentration of nitrogen rises rapidly and levels off at 680 ppm, the inlet concentration.

At this point, the catalyst bed either contains adsorbed nitrogen in equilibrium with the gas phase, or the rate of nitrogen adsorption has decreased to the point where it is immeasurable. In addition, it appears that the parahydrogen concentration in the effluent stream becomes constant.

The quantity of adsorbed nitrogen may be obtained by material balance for the time during which it was being removed from the flowing stream. For the data from Run 3, it is estimated that the nitrogen content of 5.8 cubic feet of hydrogen was adsorbed; i.e., 0.0765 grams of nitrogen per gram of catalyst.

TABLE 4

RUN NO. 3. DATA COLLECTED DURING NITROGEN ADSORPTION PERIOD

Flow of $H_2$ containing 680 ppm $N_2$

| Time Minutes from start of run | SCFM | Total flow from start SCF | Inlet concn. % p-$H_2$ | Outlet concn. % p-$H_2$ | Outlet concn. ppm $N_2$ | Flow gms $H_2$/min gm. cat. | Gms $H_2$ conv./min. gm. cat. | $\ln \frac{C_i-C_o}{C_i-C_e} \frac{C_o-C_e}{C_o-C_e}$ |
|---|---|---|---|---|---|---|---|---|
| 0 | 0.10 | 0 | 25.0 | 50.7 | 0 | 0.136 | 0.035 | - - - - |
| 10 | 0.095 | 0.952 | 25.0 | 50.7 | 0 | 0.129 | 0.0331 | - - - - |
| 20 | 0.095 | 1.897 | 25.0 | 50.6 | 0 | 0.129 | 0.0331 | 0.0472 |
| 30 | 0.095 | 2.85 | 25.0 | 50.3 | 0 | 0.129 | 0.0327 | 0.061 |
| 40 | 0.094 | 3.79 | 25.0 | 49.9 | 0 | 0.128 | 0.0319 | 0.072 |
| 50 | 0.094 | 4.73 | 25.0 | 48.5 | 0 | 0.128 | 0.030 | 0.095 |
| 55 | 0.094 | 5.21 | 25.0 | 47.4 | 15 | 0.128 | 0.0286 | 0.109 |
| 59 | 0.094 | 5.58 | 25.0 | 46.1 | 185 | 0.128 | 0.027 | 0.123 |
| 61 | 0.095 | 5.77 | 25.0 | 45.7 | 290 | 0.129 | 0.0267 | 0.126 |
| 63 | 0.095 | 5.96 | 25.0 | 45.1 | 400 | 0.129 | 0.026 | 0.132 |
| 65 | 0.095 | 6.15 | 25.0 | 44.9 | 600 | 0.129 | 0.0257 | 0.134 |
| 67 | 0.095 | 6.34 | 25.0 | 44.8 | 675 | 0.129 | 0.0255 | 0.135 |
| 70 | 0.094 | 6.62 | 25.0 | 44.8 | 680 | 0.128 | 0.0254 | 0.135 |
| 75 | 0.094 | 7.09 | 25.0 | 44.8 | 680 | 0.128 | 0.0254 | 0.135 |
| 90 | 0.095 | 8.50 | 25.0 | 44.8 | 680 | 0.129 | 0.0254 | 0.135 |
| | | | | RESIDUAL ACTIVITY AFTER NITROGEN ADSORPTION EQUILIBRIUM | | | | |
| - - | 0.044 | - - - | 25.0 | 49.3 | 680 | 0.060 | 0.015 | 0.083 |
| - - | 0.097 | - - - | 25.0 | 44.8 | 680 | 0.133 | 0.026 | 0.135 |
| - - | 0.178 | - - - | 25.0 | 39.5 | 680 | 0.255 | 0.033 | 0.180 |
| - - | 0.234 | - - - | 25.0 | 36.9 | 680 | 0.320 | 0.038 | 0.192 |

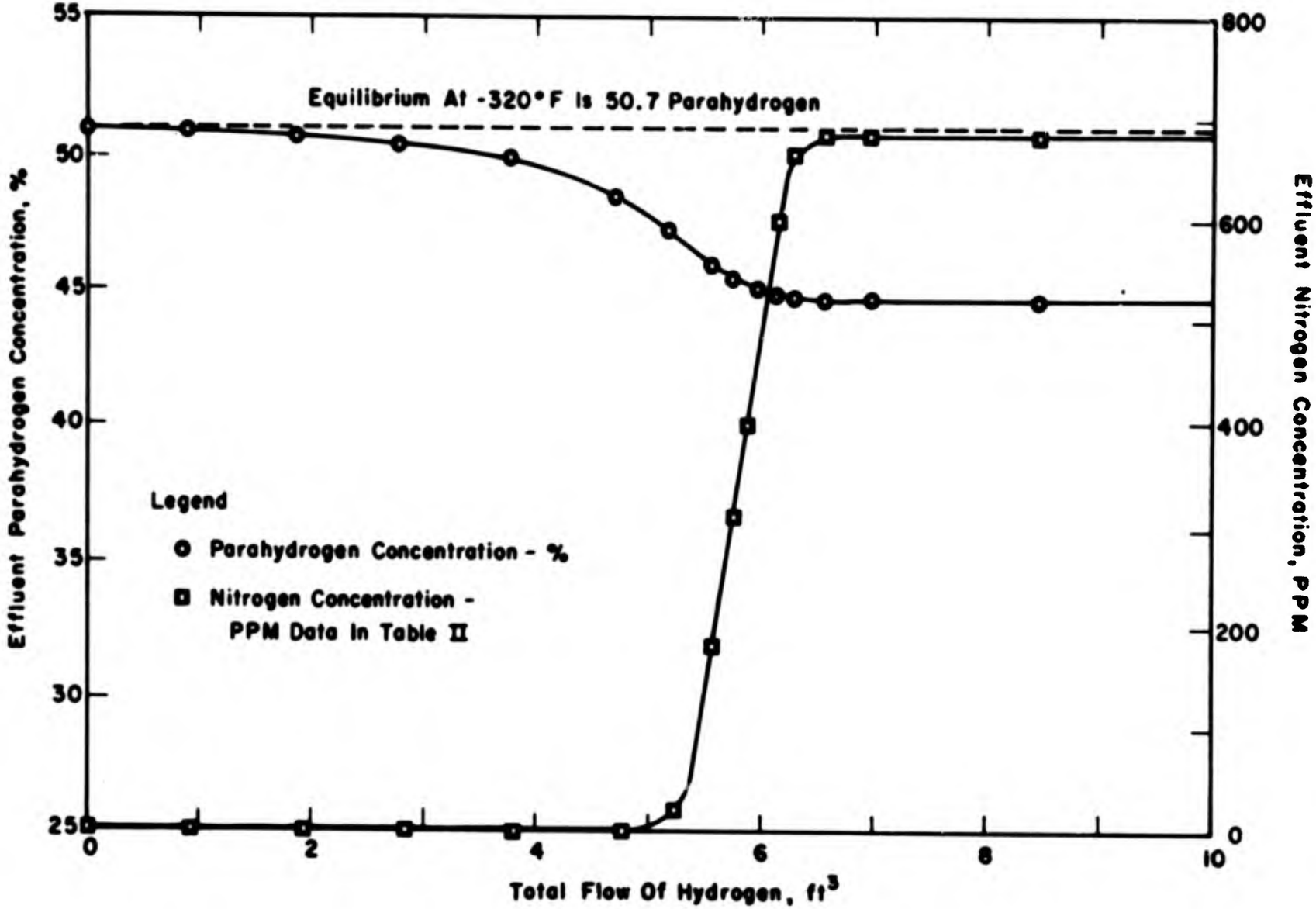


Figure 23. Effect Of Nitrogen Adsorption Upon Ortho-Parahydrogen Conversion - Run No. 3

The conversion rate steadily decreased during the period in which nitrogen was being adsorbed and appeared to become constant when the adsorption appeared complete. This can be seen in Figure 23 and is also expressed quantitatively in Figure 22. The upper line, Curve (A), represents the activity of the catalyst in an "unpoisoned" state. As nitrogen addition to the catalyst occurs, its over-all activity steadily decreases. Figure 22 shows this decrease with time as the run progresses, the points plotted corresponding to data of Table 4. When the measurable adsorption of nitrogen ceased, the activity becomes constant and corresponds to the lower line, Curve (B). The adsorption of 0.0765 gms of nitrogen per gram of catalyst has reduced its activity to 15.8% of the initial activity (for the ortho to para conversion at -320°F and 100 psig).

A total of eight runs was made with three different catalysts and at three temperatures. The catalyst type, bed size, and operating temperature and pressure are listed in Table 5. In all cases the experimental procedure and data treatment were similar to that for Run 3.

Runs 1-6 are with one catalyst exposed to two different nitrogen contaminant levels at each of three temperatures. Runs 7 and 8 are with two other catalysts exposed to a single nitrogen contaminant level at a single temperature. Table 6 lists the hydrogen flow in SCFM and in grams per minute; the parahydrogen contents at the inlet and outlet of the reactor at the start of the run before a significant quantity of nitrogen had been adsorbed, and also for the same run after the measurable rate of nitrogen adsorption had ceased; and the quantity of nitrogen adsorbed at this point, as grams of nitrogen per gram of catalyst. The quantity of nitrogen adsorbed is calculated by a material balance for nitrogen after the reactor effluent hydrogen stream exhibits the same nitrogen content as the inlet stream. The quantity of hydrogen converted per minute per gram of catalyst is computed from the known hydrogen converted per minute per gram of catalyst is computed from the known hydrogen flow and the parahydrogen concentration change in the reactor. The logarithmic mean driving force is calculated from the reactor inlet, $C_i$, and exit, $C_o$, concentrations of parahydrogen, knowing that the equilibrium concentration of parahydrogen at -297°F is 42.3%; at -320°F is 50.7%; at -345°F is 62.4%.

TABLE 5

CATALYST BED CHARACTERISTICS

| Run No. | Catalyst | Surface Area B.E.T., $m^2/gm$ | Particle Size, mesh | Catalyst Charged wt, gms | Reactor Dimensions I.D. x Length |
|---|---|---|---|---|---|
| 1 | APACHI* | 563 | 30-50 | 1.7134 | 0.25" x 6" |
| 2 | APACHI | 563 | 30-50 | 0.2568 | 0.18" x 2" |
| 3 | APACHI | 563 | 30-50 | 1.7134 | 0.25" x 6" |
| 4 | APACHI | 563 | 30-50 | 0.2568 | 0.18" x 2" |
| 5 | APACHI | 563 | 30-50 | 1.7134 | 0.25" x 6" |
| 6 | APACHI | 563 | 30-50 | 0.2568 | 0.18" x 2" |
| 7 | Iron Gel | 264 | 30-50 | 4.1071 | 0.25" x 5.5" |
| 8 | Chromia/Alumina | 137 | 1/8" x 1/8" | 50.3 | 0.75" x 5" |

* The APACHI catalyst used in the nitrogen adsorption experimentation was prepared by the Houdry Process and Chemical Company, and it is equivalent to the 1049-44 catalyst developed by Air Products and Chemicals, Inc. under Air Force Contract No. AF 33(616)-7506.

TABLE 6

CATALYST ACTIVITY BEFORE AND AFTER NITROGEN ADSORPTION

| Run No. | Period in run | Temp. °F | Press psig | PPM $N_2$ in $H_2$ feed | $H_2$ SCFM | Flow gms/min | Para $H_2$ inlet % | Concn outlet % | $N_2$ Adsorb gms $N_2$/ gms cat | Gms $H_2$ Conv Min/Gm Cat | $\frac{C_i - C_o}{\ln \frac{C_i - C_e}{C_o - C_e}}$ |
|---|---|---|---|---|---|---|---|---|---|---|---|
| 1 | start | -297 | 100 | 680 | 0.1 | 0.235 | 25.0 | 41.2 | 0.00 | 0.061 | 0.059 |
| 1 | after * | -297 | 100 | 680 | 0.1 | 0.235 | 25.0 | 38.3 | 0.047 | 0.0183 | 0.09 |
| 2 | start | -297 | 100 | 60 | 0.1 | 0.235 | 25.0 | 37.8 | 0.00 | 0.117 | 0.095 |
| 2 | after * | -297 | 100 | 60 | 0.1 | 0.235 | 25.0 | 30.5 | 0.0237 | 0.05 | 0.143 |
| 3 | start | -320 | 100 | 680 | 0.1 | 0.235 | 25.0 | 50.7 | 0.00 | 0.035 | ** |
| 3 | after * | -320 | 100 | 680 | 0.1 | 0.235 | 25.0 | 44.8 | 0.0765 | 0.025 | 0.13 |
| 4 | start | -320 | 100 | 60 | 0.1 | 0.235 | 25.0 | 43.9 | 0.00 | 0.172 | 0.142 |
| 4 | after * | -320 | 100 | 60 | 0.1 | 0.235 | 25.0 | 31.3 | 0.0465 | 0.0576 | 0.223 |
| 5 | start | -345 | 100 | 680 | --- | ----- | 25.0 | ---- | 0.00 | ----- | ----- |
| 5 | after * | -345 | 100 | 680 | 0.1 | 0.235 | 25.0 | 46.4 | 0.1065 | 0.0293 | 0.265 |
| 6 | start | -345 | 100 | 60 | 0.1 | 0.235 | 25.0 | 51.1 | 0.00 | 0.238 | 0.218 |
| 6 | after * | -345 | 100 | 60 | 0.1 | 0.235 | 25.0 | 30.2 | 0.0765 | 0.0475 | 0.35 |
| 7 | start | -320 | 100 | 680 | 0.288 | 0.68 | 25.0 | 46.9 | 0.00 | 0.036 | 0.114 |
| 7 | after * | -320 | 100 | 680 | 0.1 | 0.235 | 25.0 | 42.4 | 0.031 | 0.0100 | 0.154 |
| 8 | start | -320 | 100 | 680 | 0.1 | 0.235 | 26.5 | 43.7 | 0.00 | 0.00081 | 0.139 |
| 8 | after * | -320 | 100 | 680 | 0.1 | 0.235 | 25.0 | 30.7 | 0.014 | 0.000197 | 0.22 |

* $N_2$ adsorption

** indeterminate

The amount of nitrogen adsorbed at equilibrium for each test condition is related to the B. E. T. surface area in Table 7. It is assumed in computing that catalyst area which remains in an "uncovered" state that all of the adsorbed nitrogen is present in a layer not more than one molecule thick and that the area of an adsorbed nitrogen molecule is $14°A^2$. The catalyst activity expressed as a percent of the original activity is listed in Table 7.

The relationship between the portion of the original catalyst B.E.T. surface not covered with adsorbed nitrogen and the residual catalytic activity is presented in Figure 24. If the reduction in ortho-parahydrogen conversion activity were directly related to the reduction in B.E.T. surface due to nitrogen adsorption, the diagonal straight line would represent the nitrogen adsorption effect. It is seen that the fall off in activity is much greater than such a linear effect. A coverage of 50% of the catalyst with nitrogen reduces the activity to about 10% of the original; a coverage of 25% reduces the activity to 20% of the original; a coverage of 10% of the surface reduces the activity to about 30% of the original. It may also be noted that the curve of Figure 5 empirically correlates the effect of adsorbed nitrogen upon three different catalysts which vary greatly in B.E.T. surface area and in intrinsic activity.

The adsorption capacity values listed in Table 6 are plotted in Figure 25 in accordance with a Polanyi type correlation, the data for this correlation being developed in Table 8. The density of the adsorbed phase is assumed to be the same as that for liquid nitrogen at the temperature involved, namely 0.744 gms/cc at -297°F, 0.806 gms/cc at -320°F, and 0.866 gms/cc at -345°F. Figure 25 is included principally to show the consistency of the adsorption capacity measurements and to present the capacity differences for the three catalysts.

## E. THEORETICAL INTERPRETATION OF EXPERIMENTAL RESULTS

The ortho-parahydrogen conversion at lower temperatures occurs by the interaction between an inhomogeneous magnetic field and the magnetic field associated with the nuclear spin of the hydrogen nuclei. Since the magnetic field is produced along the axis of rotation of the spinning nucleus, an external field which causes a reversal of the direction of this nuclear magnetic field, in effect, produces a reversal of spin in one

## TABLE 7

## CATALYST ACTIVITY RELATED TO SURFACE AREA COVERED WITH NITROGEN

| Run No. | Initial catalyst area $m^2/gm$ | Gms $N_2$ adsorbed per gm catalyst | Catalyst area remaining, % of original | Catalyst Activity, % of original |
|---|---|---|---|---|
| 1 | 563 | 0.047 | 75.0 | 19.7 |
| 2 | 563 | 0.0237 | 87.3 | 28.4 |
| 3 | 563 | 0.0765 | 60.5 | 15.8 |
| 4 | 563 | 0.0465 | 75.1 | 21.3 |
| 5 | 563 | 0.1065 | 43.2 | 9.2 |
| 6 | 563 | 0.0765 | 59.1 | 12.4 |
| 7 | 264 | 0.031 | 64.7 | 20.6 |
| 8 | 137 | 0.014 | 69.3 | 15.4 |

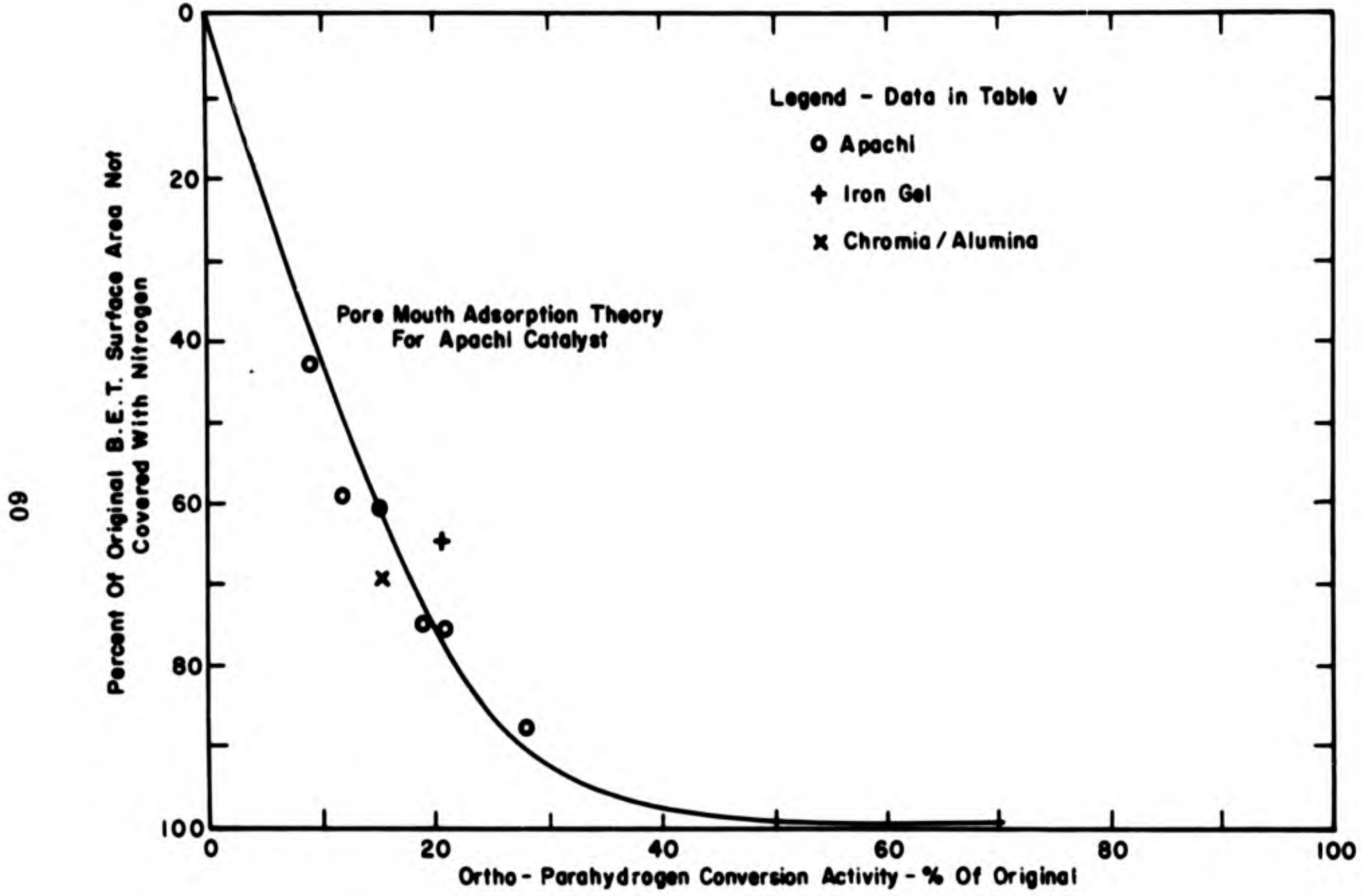


Figure 24. Relationship Between Ortho - Parahydrogen Conversion Activity And Nitrogen Adsorption

TABLE 8

ADSORPTION DATA IN TERMS OF POLANYI-TYPE VARIABLES

| Run No. | Nitrogen Adsorbed | | RT ln $P_o/P$ |
|---|---|---|---|
| | Gms $N_2$/gm. cat. | CC $N_2$/gm. cat. | |
| 1 | 0.047 | 0.0632 | 1170 |
| 2 | 0.0237 | 0.0318 | 1610 |
| 3 | 0.0765 | 0.095 | 805 |
| 4 | 0.0465 | 0.0577 | 1180 |
| 5 | 0.1065 | 0.123 | 408 |
| 6 | 0.0765 | 0.0883 | 715 |
| 7 | 0.031 | 0.0384 | 810 |
| 8 | 0.014 | 0.0174 | 810 |

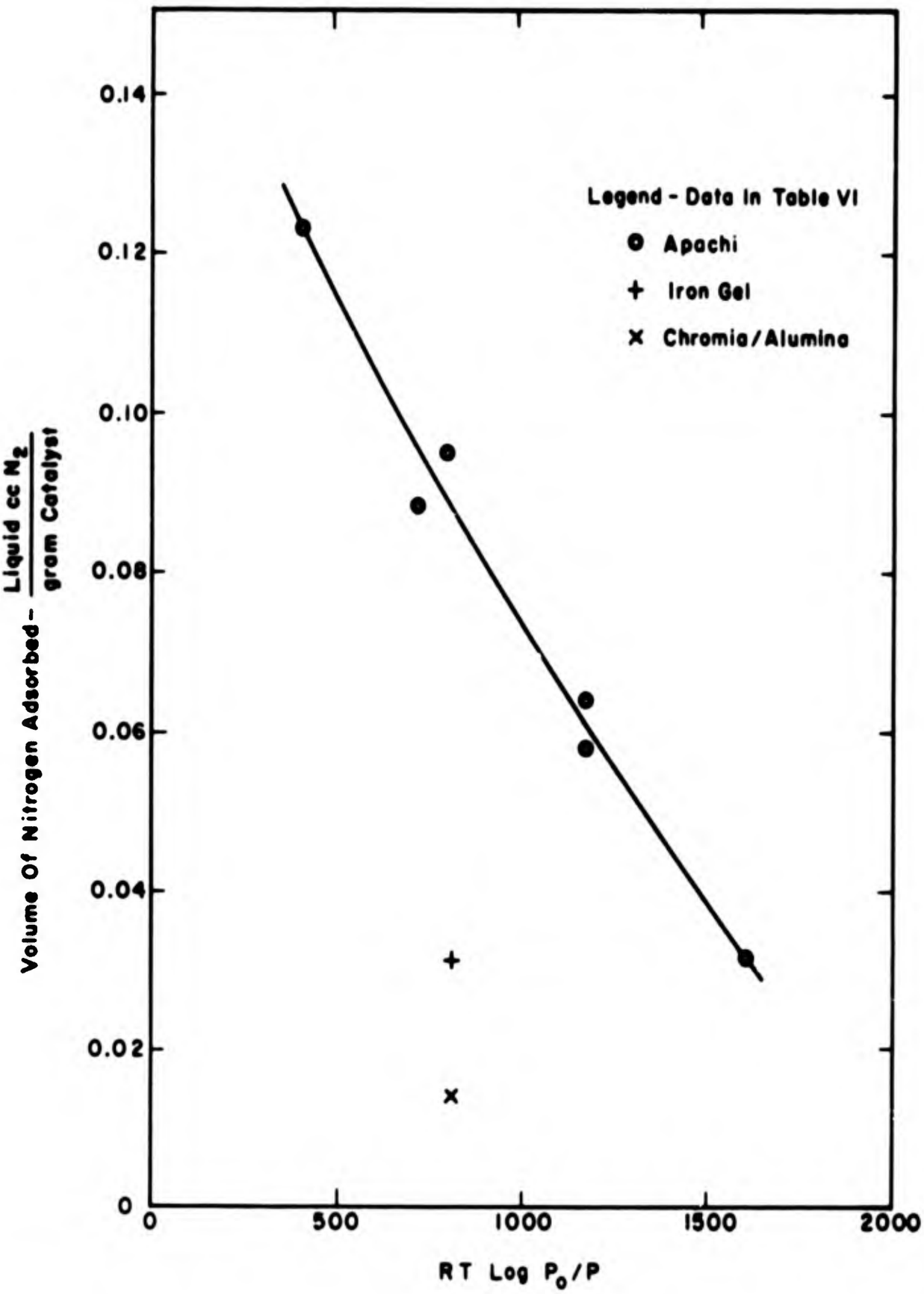


Figure 25. Nitrogen Adsorption Polanyi -Type Correlation

of the nuclei. This spin reversal is equivalent to an ortho-para transition. The external field may be any inhomogeneous field of molecular dimensions. In the case of the solid catalysts, the catalytic effect is ascribed to the influence of the inhomogeneous field of the paramagnetic component of the catalyst upon the physically adsorbed hydrogen (3, 5). Several papers by Weitzel et al (6, 7, 8, 9, 10, 11) concerned with catalyst evaluation and kinetic studies in dynamic streams provide background information.

The catalyst is active because of a combination of high physical adsorptive capacity for hydrogen, a high concentration of magnetic specie and a high paramagnetic susceptibility.

The effect of adsorbed nitrogen can possibly be explained in light of one of two theories: (1) the nitrogen may be readily adsorbed at the pore mouths, thereby greatly increasing the pore diffusional resistance and thus lowering the catalyst activity; and (2) the "active sites" which bring about most of the ortho-parahydrogen conversion may be the sites which preferentially adsorb nitrogen.

1. Pore Mouth Contamination Theory

At the boiling point of an adsorbate, the process of physical adsorption becomes similar to the phase change of condensation. Consequently, an adsorbate in a gas stream would tend to "adsorb" or "condense" on the closest cold surface, and the "adsorptive capacity" of an adsorbent for an adsorbate is very high at this temperature. The nitrogen contamination studies were conducted near the boiling point of nitrogen, and the closest cold surface to the flowing hydrogen stream in the reactor was the catalyst surface just within the pore mouths.

In addition, Figure 22 indicates that the adsorption of nitrogen may have caused a switch from a bulk mass transfer, pore diffusion, and surface reaction combined limitation (S-shaped curve) to a pore diffusion and surface reaction controlled situation (straight line going through the origin). This change could only occur by a decrease in the bulk diffusional resistance or an increase in the surface reaction and pore diffusion resistances. The present of small quantities nitrogen in the reactant stream could not greatly alter the bulk diffusional characteristics

of the system; but the adsorption of nitrogen within the pore mouths could increase the pore diffusion and surface reaction resistances.

These two facts led to the theoretical analysis of the effect of nitrogen adsorption at the pore mouths. The analysis assumed that all of the nitrogen was adsorbed in a monolayer at the pore mouths. This adsorption would decrease the area available for catalysis, decrease the free cross sectional area of the pores, and greatly decrease the reactant concentration gradient within the pores. All of these would, in turn, decrease the rates of pore diffusion and surface reaction, and thus lower the catalyst activity.

Figure 24, a graph of surface area not covered by nitrogen versus conversion activity, compares the theoretical results of the pore mouth adsorption study with the actual experimental data. The average deviation between the theoretical and experimental results was less than 4%.

The derivation of the pore mouth contamination theory, and its application to the nitrogen contamination case, are presented in Appendix III.

2. Active Site Adsorption Theory

The basis of a widely-followed theory of catalysis, first proposed by H. S. Taylor, is the postulation that a relatively small portion of a catalyst's surface area - the "active sites" - is responsible for most of the catalytic activity. The effect of adsorbed nitrogen may be viewed in this light.

The "active sites" which bring about most of the ortho-parahydrogen conversion may also be the sites which preferentially adsorb nitrogen. Such adsorbed nitrogen would drastically reduce the catalyst activity. The data presented in Figure 22 suggests that the loss in activity is exponentially related to the fraction of catalyst surface which is covered with adsorbed nitrogen. It appears that the loss in catalytic activity as a function of surface coverage by nitrogen is similar to the decrease in the differential heat of adsorption as a function of coverage, which is related to the site energy distribution. Further theoretical and experimental work is needed to evaluate this theory.

# IV. CATALYST DEVELOPMENT

## A. IMPROVEMENTS TO THE APACHI CATALYSTS

An intensive statistical investigation of the preparation variables of the APACHI system of catalysts was conducted. The objective was to find the preparation technique yielding a catalyst of maximum activity. This investigation succeeded in raising the activity of the APACHI catalyst system from 9.7 to 13.7 times the standard iron gel activity. Details of the optimum preparation technique are reported in Reference (12).

The test results of the most active catalyst, 1130-40-2, and the second most active catalyst, 1070-101 are shown in Table 9, with the iron gel data shown for reference. The data are shown in graphical form in Figures 26 and 27.

## B. SUPERPOROUS CATALYSTS

A new, low density, high surface area, inert support material has been prepared. The support had a surface area of 825 square meters per gram, a density of approximately 5 pounds per cubic foot, an estimated pore volume of 36 cubic centimeters per gram, and a calculated average pore diameter of 1700° A.

Incorporation of a promoter on this superporous support would result in a unique catalyst with large pores and a high surface area. Normally, surface area is a reciprocal function of pore diameter. When the chemical reaction resistance is decreased by increasing the surface area on which the reaction can take place, the resistance due to pore diffusion is increased by the corresponding decrease in pore diameter. However, with this new support material, this reciprocal physical effect will be greatly diminished, and optimization will be limited by the chemical characteristics of the catalyst alone.

This new effort is presently in the preliminary stage but the results are very encouraging. The first attempt at incorporating a promoter on this support resulted in a catalyst with an activity 4.5 times that of the standard iron oxide gel.

BLANK PAGE

## TABLE 9

### ORTHO-PARAHYDROGEN CONVERSION DATA FOR APACHI CATALYSTS* STANDARD IRON GEL CATALYST AND AN ADVANCED CATALYST

| Catalyst Number | Catalyst Weight (Gms) | Flow Rate (SCFM) at 70° F | Gms $H_2$/Min / Gms. Cat. | Feed Concentration (% Para - $H_2$) | Effluent Concentration (% Para - $H_2$) | Fraction Concerted $C_i - C_e$ | Gms Converted/Min / Gms. Cat. | $\frac{C_i - C_o}{\ln \frac{C_i - C_e}{C_o - C_e}}$ |
|---|---|---|---|---|---|---|---|---|
| 1130-40-2 | 0.1845 | 0.0398 | 0.504 | 25.0 | 50.4 | 0.254 | 0.128 | 0.058 |
| 50 - 80 mesh | gms. 1/8" | 0.0901 | 1.142 | 25.0 | 49.4 | 0.244 | 0.278 | 0.083 |
| Activation @ | ID x 4" | 0.1531 | 1.943 | 25.0 | 47.5 | 0.225 | 0.437 | 0.111 |
| 300° C with $N_2$ | chamber | 0.2181 | 2.770 | 25.0 | 45.5 | 0.200 | 0.554 | 0.130 |
| | | 0.2799 | 3.542 | 25.0 | 43.7 | 0.187 | 0.662 | 0.151 |
| 1070-101 | 0.1871 | 0.0479 | 0.598 | 25.2 | 50.1 | 0.257 | 0.154 | 0.053 |
| 70-80 mesh | 1/8" I.D. | 0.1052 | 1.315 | 25.4 | 48.7 | 0.233 | 0.307 | 0.092 |
| Activation at | x 4" | 0.1546 | 1.930 | 25.4 | 47.2 | 0.218 | 0.420 | 0.111 |
| 300° C with $N_2$ | chamber | 0.1962 | 2.450 | 25.4 | 46.0 | 0.206 | 0.505 | 0.123 |
| 20-5 | 0.5812 | 0.0493 | 0.199 | 25.8 | 46.5 | 0.207 | 0.0412 | 0.122 |
| 70 - 80 mesh | 1/8" ID | 0.0775 | 0.313 | 25.9 | 42.5 | 0.166 | 0.0520 | 0.151 |
| Activation at | x 2-1/2" | 0.1082 | 0.435 | 26.1 | 39.6 | 0.135 | 0.0587 | 0.170 |
| 100° C with $H_2$ | chamber | 0.1956 | 0.789 | 26.3 | 34.6 | 0.083 | 0.0655 | 0.198 |

*Conversion at 100 psig and -320° F

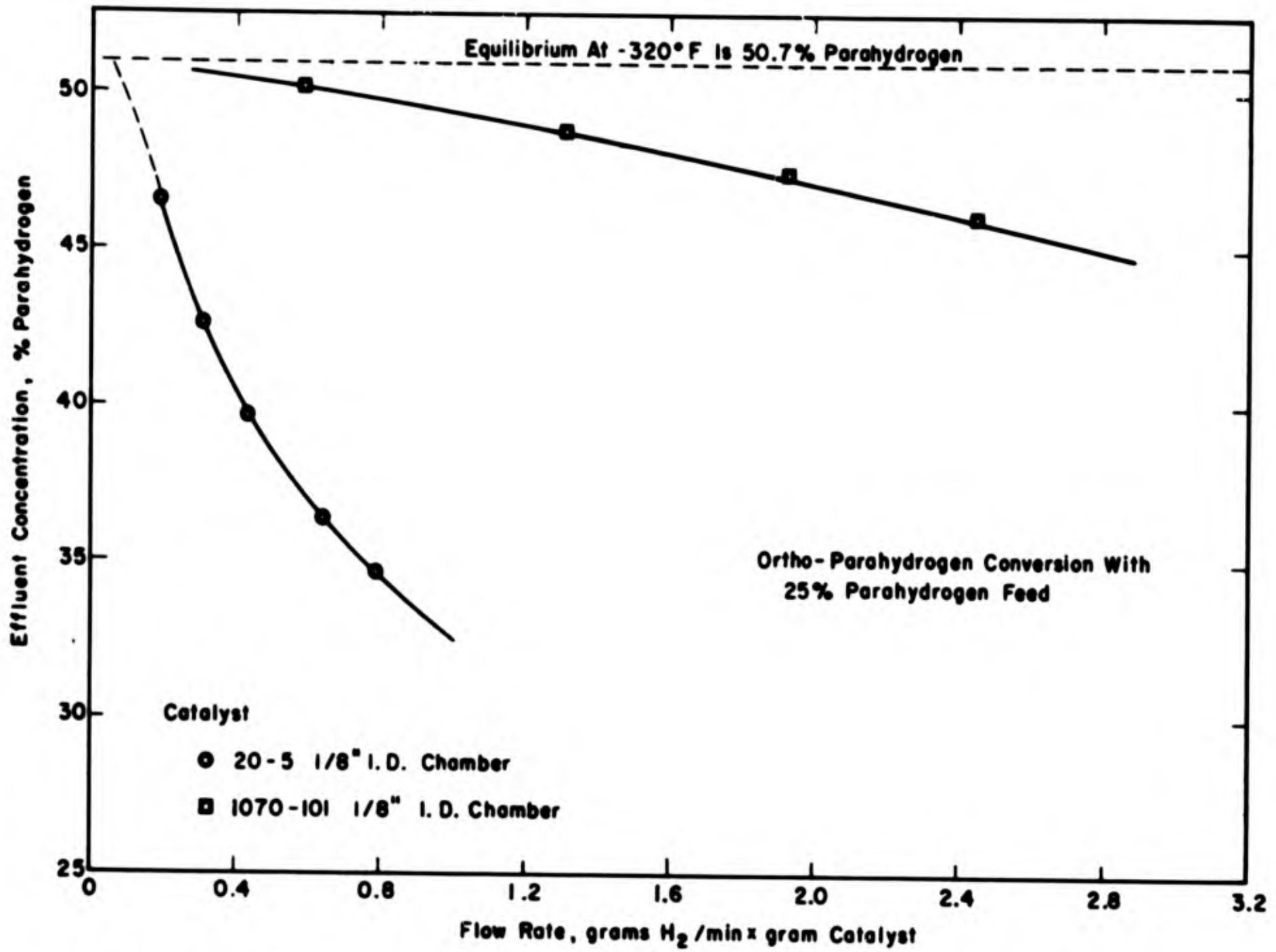


Figure 26. Experimental Conversion Ratio Versus Hydrogen Flow Rate

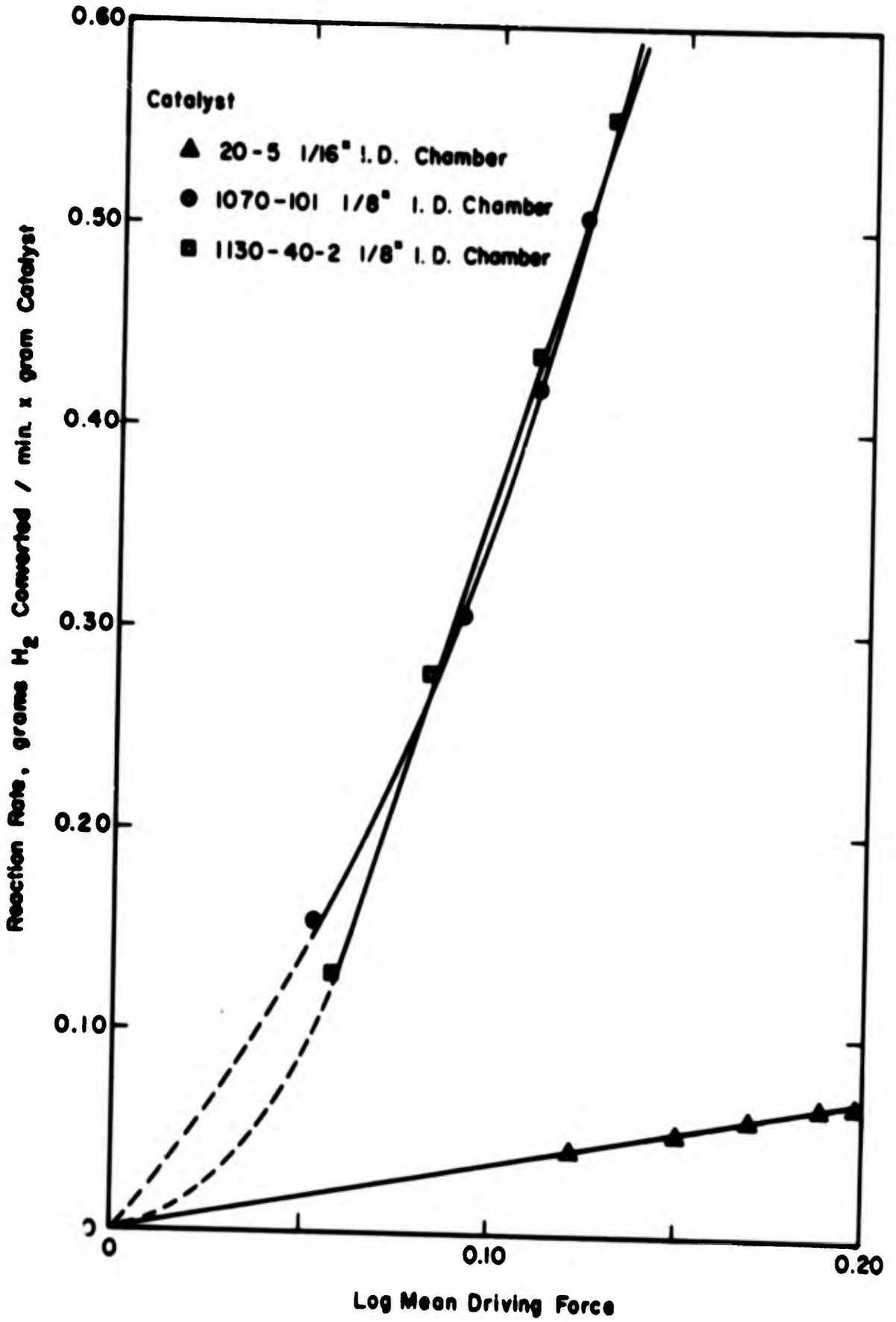


Figure 27. Experimental Conversion Rate Versus Log Mean Driving Force

## C. BORIC ACID IMPREGNATED APACHI CATALYSTS

Arthur D. Little, Inc. (13) reports that the activity of an APACHI catalyst is improved by soaking it in a boric acid solution.

Air Products has taken one of its best preparations (No. 1070-80) and impregnated it with boric acid. The untreated catalyst had an activity of 9.0 times the iron gel standard while after treatment, an activity of 6.2 was measured when activated at 250° C.

Arthur D. Little, Inc. received a sample of APACHI catalyst (1014-10-2) from the Air Force. The activities which they measured were 6.2 and 8.7, before and after boric acid impregnation, respectively. The final activity of 8.7 is the same value that Air Products obtained for an untreated sample of 1014-10-2, which was activated with the established Air Products' procedure. Consequently, APCI believes that the Arthur D. Little, Inc. measurements were made on samples which were not sufficiently activated.

## D. EVALUATION OF CATALYSTS PREPARED BY ENGLEHARD INDUSTRIES, INC.

At the request of the Aeronautical Systems Division, APCI tested three proprietary catalysts submitted by Englehard Industries, Inc., Newark, New Jersey. The evaluations were conducted on February 11, 1963, in the Air Products' para-orthohydrogen conversion facility, Emmaus, Pennsylvania, and were viewed by representatives of Englehard Industries, Inc.

The three catalysts were activated by purging with a 2.0 SCFH hydrogen stream at 300°C for one to two hours. The activities of the samples were determined by APCI personnel using the procedure established for all catalyst evaluations performed under this contract. Table 10 is a summary of the data from these tests, and Figure 28 shows these data in plotted form in comparison to the standard iron gel catalyst.

TABLE 10

ORTHO-PARAHYDROGEN CONVERSION DATA FOR THE ENGLEHARD CATALYSTS*

| Catalyst Number | Sample Weight (Gms) | Flow Rate (SCFM) at 70° C | Gms $H_2$/Min | | Concentration | | Activation |
|---|---|---|---|---|---|---|---|
| | | | Gm | Cat. | Feed (% Para-$H_2$) | Effluent (% Para-$H_2$) | |
| Englehard C-3090 | 3.6060 | 0.0665 | 0.0432 | | 25.5 | 25.9 | 300°C 2.75 hrs. $H_2$ gas |
| Englehard C-3091 | 3.1998 | 0.0614 | 0.0449 | | 25.5 | 50.0 | 300°C 1.0 hr. $H_2$ gas |
| | | 0.1229 | 0.0902 | | 25.5 | 47.8 | |
| | | 0.2206 | 0.160 | | 25.5 | 43.9 | |
| | | 0.3171 | 0.232 | | 25.5 | 40.4 | |
| Englehard C-3093 | 3.5044 | 0.0731 | 0.0488 | | 25.5 | 44.6 | 300°C 1.0 hr. $H_2$ gas |
| | | 0.1543 | 0.103 | | 25.5 | 37.4 | |
| | | 0.2956 | 0.195 | | 25.5 | 32.5 | |
| 20-5 (70-80 mesh) | 0.5812 | 0.0493 | 0.199 | | 25.8 | 46.5 | |
| | | 0.0775 | 0.313 | | 25.9 | 42.5 | |
| | | 0.1082 | 0.435 | | 26.1 | 39.6 | |
| | | 0.1605 | 0.645 | | 26.3 | 36.3 | |
| | | 0.1956 | 0.789 | | 26.3 | 34.6 | |

* Conversion at 100 psig and -320° F.

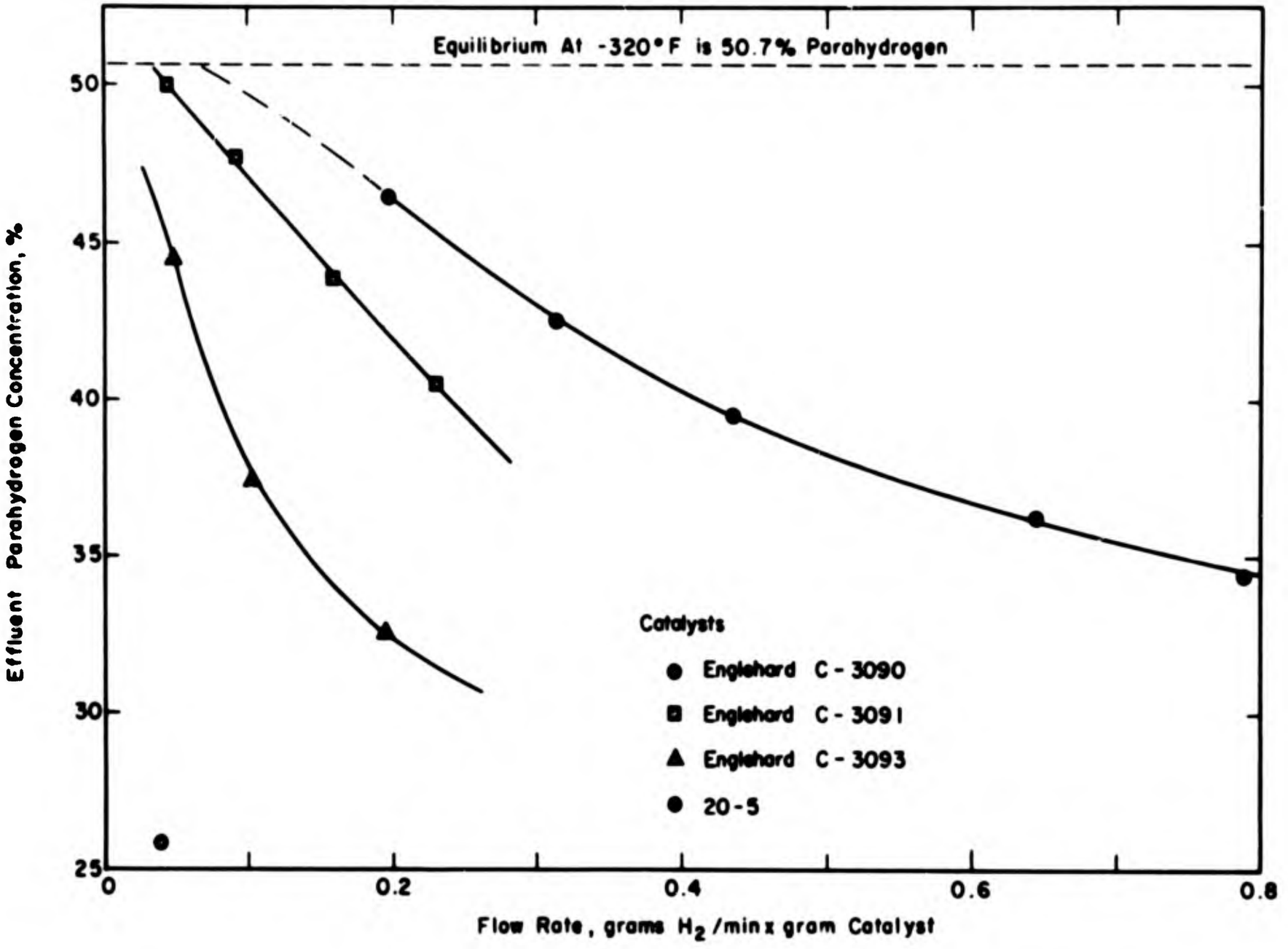


Figure 28. Comparison Of Englehard Catalysts And Standard Iron Gel

The measured activities of Englehard C-3090, C-3093, and C-3091 (compositions undisclosed) were 0.01, 0.24, and 0.57 times the standard iron gel catalyst, resprectively, and consequently only 0.001, 0.024, and 0.057 times the activity of 1049-100 APACHI catalyst.

## V. RECOMMENDATIONS FOR FURTHER WORK

Additional improvements in the APACHI series of catalyst are possible through further manipulation of the preparational variables. This optimum system can now be arrived at through a relatively small number of experiments due to the improved understanding of the conversion mechanisms.

Further mechanism studies are recommended to reduce the semi-quantitative results reported herein to a more precise model. Activity in this area will lend significant support to the catalyst optimization experiments. A significant part of the mechanism studies should be concerned with the elucidation of the catalyst poisoning phenomena. These studies would serve a two-fold purpose: poisoning serves as a tool for identifying certain phenomena limiting the catalysts performance under normal operations; and the poisoning phenomena needs to be understood so that maximum contaminant levels in the hydrogen being processed can be specified.

The superporous substrate evolved under this program shows a number of unusual properties which indicate that it may lend itself to the development of a catalyst system superior to the present APACHI system. Additional studies aimed at solving the problems associated with establishing an active promoter on the surface of this structure are recommended.

## VI. CONCLUSIONS

A catalyst has been developed for promoting the low temperature para-ortho reaction of hydrogen which is 13.7 times more effective than iron gel, the best commercially available material. The results of an earlier program carried out by Air Products produced a catalyst 9.7 times more effective than the iron gel.

A complex mechanism describing the conversion has been postulated based on mass transfer and reaction rate limitations. While the model has not yet been reduced to a completely quantitative form, it successfully explains the kinetics of the conversion reaction over a wide range of flow rate, pressure, and catalyst particle size.

An extensive experimental and theoretical analysis of catalyst poisoning has resulted in data which can be explained on the basis of the blocking of the catalyst pores with the contaminant. The possibility still exists, however, that the reduced activity is due to preferential adsorption of contaminant on the most active conversion sites on the catalyst.

## REFERENCES


1. Langmuir, J., "The Adsorption of Gases on Plane Surfaces of Glass, Mica, and Platinum", J. Am. Chem. Soc. 40, 1361 (1918)

2. Air Products and Chemicals, Inc., Allentown, Pennsylvania, Singleton, A. H., G. E. Kinard, R. W. Waring, Jr., and A. Lapin: "The Application of the Para-Ortho Conversion Reaction of Hydrogen to Orbital Systems", Summary Technical Report, Contract AF 33 (657)-10057, February 1964.

3. Air Products and Chemicals, Inc., Allentown, Pennsylvania: Clark, R. G., J. F. Kucirka, A. Jambhekar, and G. E. Schmauch: "Investigation of the Para-Ortho Shift of Hydrogen", Summary Technical Report ASD TDR 62-833, Contract No. AF 33 (616) - 7506, July 1962.

4. Keeler, R. N. and K. D. Timmerhaus, "Poisoning and Reactivation of Ortho-Parahydrogen Conversion Catalyst", Advances in Cryogenic Engineering, 4, K. D. Timmerhaus, ed., Plennum Press, New York, 1960, pp. 296-306.

5. Farkas, L. and L. Sandler, "The Heterogeneous Ortho-Para-conversion on Paramagnetic Crystals", J. Chem. Phys., 8, 248-251 (1940).

6. Barrick, P. L., D. H. Weitzel, and T. W. Connolly, "Ortho-Parahydrogen Conversion Studies", Advances in Cryogenic Engineering Conference, 1, K. D. Timmerhaus, ed., Plennum Press, New York, 1960, pp. 285-290.

7. Weitzel, D. H., J. W. Draper, O. E. Park et al, "Catalysis of the Ortho-Parahydrogen Conversion", Advances in Cryogenic Engineering Conference, 2, K. D. Timmerhaus, ed., Plennum Press, New York, 1960, pp. 12-18.

8. Weitzel, D. H., W. V. Loebenstein et al, "Ortho-Para Catalysis in Liquid-Hydrogen Production", J. Res. N. B. S., 60, 221-227 (1958).

9. Weitzel, D. H., C. C. Van Valin and J. W. Draper, "Design Data for Ortho-Parahydrogen Converters", Advances in Cryogenic Engineering Conference, 3, K. D. Timmerhaus, ed., Plennum Press, New York, 1960, pp. 73-84.

## REFERENCES (Cont'd.)

10. Weitzel, D. H., J. H. Blake, and M. Konecnik, "Flow Conversion Kinetics of Ortho and Parahydrogen", Advances in Cryogenic Engineering Conference, 4, K. D. Timmerhaus, ed., Plennum Press, New York, 1960, pp. 286-295.

11. Keeler, R. N., D. H. Weitzel, J. H. Blake and M. Konecnik, "A Kinetics Study of Ortho-Para Hydrogen Conversion", Advances in Cryogenic Engineering Conference, 5, K. D. Timmerhaus, ed., Plennum Press, New York, 1960, pp. 511-517.

12. Air Products and Chemicals, Inc., Allentown, Pennsylvania, Letter Report No. 7 to September 15, 1963, Contract AF 33 (657) - 10333 (Confidential Report).

13. Arthur D. Little, Inc., Cambridge, Massachusetts: "Radiation Activation of Para-Ortho Hydrogen Catalysts", Quarterly Progress Report No. 3, Contract No. AF 33 (657) - 8878, April 1963.

# APPENDIX I

## BULK DIFFUSION

When a gas is flowing through a bed of catalyst particles, a boundary layer or laminar film is formed around each particle. In this film, transport of the reactant from the bulk liquid to the external surface of the catalyst is mainly by molecular motion. The thickness of this film and therefore the average diffusion path, is directly related to the degree of turbulence in the system.

A rigorous analysis of bulk diffusion would consist of the solution of the partial differential equation which would result from setting up a microscopic mass balance on the system. However, since the velocity gradients within a packed bed are extremely difficult to characterize mathematically, a truly rigorous solution has never been completed. Thus, a less rigorous, but calculable, approach — the usual driving force method — was used. The reaction considered was the ortho to para transition; but the results, with minor modifications, can be applied to the para-ortho shift. In this method, the rate is equated to the driving force times a proportionality constant:

$$r = kA\,(C - C_s) \qquad (I - 1)$$

where $r$ = rate of mass transfer,

$$\frac{\text{gm. moles O-H}_2\text{ transferred}}{\text{sec x gm. cat.}}$$

$k$ = mass transfer coefficient,

$$\frac{\text{gm. moles O-H}_2\text{ transferred}}{\text{sec x cm}^2\text{ x }\dfrac{\text{gm. mole O-H}_2}{\text{cm}^3}}$$

$A$ = external surface area of catalyst, $\text{cm}^2/\text{gm. cat.}$

$C$ = ortho hydrogen concentration in the bulk gas stream, $\dfrac{\text{gm. moles}}{\text{cm}^3}$

$C_s$ = ortho hydrogen concentration at the catalyst surface, $\text{gm. moles/cm}^3$

The mass transfer coefficient in the above expression can be measured experimentally or estimated by using the empirical correlation derived by Thodos and coworkers *

$$k = 1.82 \frac{G}{P_N}\left(\frac{\mu}{\rho D}\right)^{-0.66}\left(\frac{d_p \rho V_s}{\mu}\right)^{-0.51} \qquad (I - 2)$$

where $G$ = superficial molar flow rate, $\frac{\text{gm. moles}}{\text{cm}^2 \times \text{sec.}}$

$P_N$ = partial pressure or non-diffusing component in the film, atm.

$\mu$ = viscosity of gas, gm./cm x sec.

$\rho$ = density of gas, $\text{gm/cm}^3$

$D$ = diffusivity of ortho hydrogen in hydrogen, $\text{cm}^2/\text{sec.}$

$d_p$ = catalyst particle diameter, cm.

$V_s$ = superficial gas velocity in reactor, cm/sec.

It can be seen from this expression that an increase in gas velocity results in an increase in the mass transfer coefficient.

Consider a tubular reactor packed with W grams of catalyst, through which hydrogen is passed at a molar flow rate of F gram moles per second. If a material balance on the orthohydrogen in the stream is made across a differential segment dW, the result will be a differential equation depicting the conversion of ortho hydrogen in the reactor.

| Rate of input of ortho hydrogen into segment dW | — | Rate of output of ortho hydrogen from segment dW | — | Rate of ortho hydrogen conversion in segment dW | = | Rate of ortho hydrogen accumulation in dW |
|---|---|---|---|---|---|---|

Figure I - 1 is a flow diagram of the system.

---

* Gamson, Thodos, and Hougen, Trans. Am. Inst. Ch. E., 39, 1, (1943)

BLANK PAGE

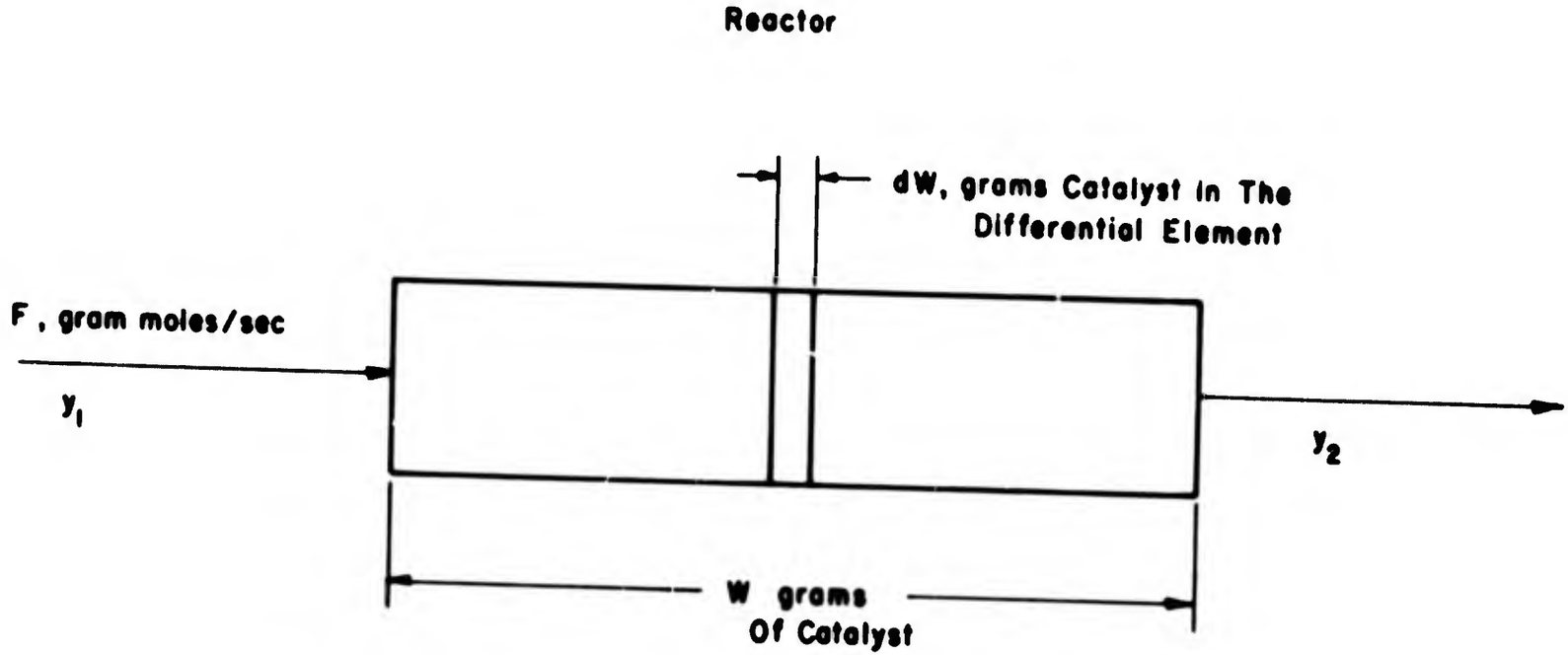


Assumption: Gas Passes Through The Reactor In Plug Flow

Figure I-1. Flow Diagram Of Ortho-Para Hydrogen Conversion Reactor

Once the system has reached steady state, the rate of accumulation at any point would be zero. Thus, the resulting material balance for steady state is:

$$r_o dW = -F dy \qquad \text{(I - 3)}$$

where $y$ = orthohydrogen mole fraction in the bulk gas stream at some point within the reactor

$F$ = molar flow rate, gram moles/sec.

$W$ = mass of catalyst in reactor, grams.

$r_o$ = overall reaction rate, at an ortho hydrogen mole fraction of y, $\frac{\text{gram moles}}{\text{sec x gm cat.}}$

If the ortho hydrogen mole fraction in the gas stream at the inlet is $y_1$ and at the outlet, $y_2$, Equation (I - 3) can be integrated between these limits to obtain:

$$\int_0^W \frac{dW}{F} = -\int_{y_1}^{y_2} \frac{dy}{r_o}$$

$$\frac{W}{F} = \int_{y_2}^{y_1} \frac{dy}{r_o} \qquad \text{(I - 4)}$$

So far, the only assumptions made in the derivation of Equation (I - 4) are as follows: plug flow and steady state. No restrictions were made to define $r_o$, the overall conversion rate. If the transport of ortho hydrogen from the bulk gas stream to the catalyst external surface limited the overall process, then the rates of the other six steps would be much larger than r, the bulk diffusion rate, and could be neglected in Equation (I - 4). In addition, the concentration of ortho hydrogen on the surface of the catalyst would be $C_e$, the equilibrium concentration at temperature T. Thus, $r_o = r = kA(C - C_e)$. By using the perfect gas law, the concentrations can be converted to mole fractions.

$$r = kA \frac{P}{RT}(y - y_e) \qquad \text{(I - 5)}$$

where $P$ = total pressure, atm.

$T$ = temperature, $^{o}K$

$R$ = gas constant, $\frac{\text{atm x cm}^3}{\text{gram moles x K}^o}$

Referring to Equation (I - 2), the generalized expression for the mass transfer coefficient k, the first approximation for $P_N$ in this equation is:

$$P_N = P \text{ (average mole fraction of parahydrogen in the film)}$$

$$= P\ (1 - y_{film})$$

$$y_{film} = 1/2\ (y + y_e)$$

$$P_N = P\ (1 - y/2 - y_e/2)$$

At a constant temperature, pressure, and catalyst particle diameter, the remainder of Equation (I - 2) is constant or a function of gas flow rate alone. Thus

$$k = \frac{C}{P\ (1\text{-}1/y\ \text{-}1/2y_e)}\ \emptyset\ (F) \qquad (I - 6)$$

where $C$ = constant
$\emptyset\ (F)$ = function of gas flow rate

Substitution of Equations (I - 5) and (I - 6) into Equation (I - 4) results in

$$\frac{W}{F} = \int_{y_2}^{y_1} \frac{P\ (1 - 1/2\ y - 1/2\ y_e)\ \ RT\ dy}{C\ \emptyset\ (F)\ AP\ (y - y_e)}$$

Integrating this expression between the stated limits:

$$\frac{W}{F} = \frac{1}{k_F} \left[ (1 - y_e)\ \ln \frac{y_1 - y_e}{y_2 - y_e} + \frac{1}{2}\ (y_2 - y_1) \right]$$

where $k_F = \frac{CA\ \emptyset\ (F)}{RT}$ = function of flow rate alone for a given catalyst and a constant temperature and pressure.

Inversion of this equation, multiplication of both sides by $(y_1 - y_2)$, and further algebraic manipulations result in the final expression:

$$\text{Observed rate of conversion, } \frac{\text{gram moles}}{\text{sec x gram cat}} = \frac{F(y_1-y_2)}{W} = \frac{k_F\,(\text{LMDF})}{1 - y_e - \frac{1}{2}\,(\text{LMDF})}$$

where LMDF = log mean driving force $= \dfrac{y_1 - y_2}{\ln \dfrac{y_1 - y_e}{y_2 - y_e}}$

For the APCI ortho-para hydrogen conversion apparatus, it can be shown that an increase in flow rate results in an increase in LMDF. Thus, $k_F$ would increase as LMDF increased. Consequently, if bulk mass transfer limited the overall process, the relationship of the observed rate with the LMDF would be much stronger than direct proportionality; in essence, a straight line extrapolation of data presented in a rate versus LMDF graph would not go through the origin.

# APPENDIX II

## PORE DIFFUSION

An exact solution for the case when the diffusion of the reacting species into the catalyst pores limits the over-all rate of conversion is extremely complicated. Any analysis is limited by the lack of diffusivity data and by the fact that it is impossible to mathematically characterize the pore structure.

### A. PRELIMINARY PORE DIFFUSION MODEL

The bases of the first approximation of the model is as follows: the ortho to parahydrogen transition can be represented by a 1st order, reversible rate expression; the catalyst consists of n smooth, cylindrical pores per gram, each with a radius r and a length L; and uniform spherical catalyst particles.

The derivation led to the following expression:

$$R_r = \frac{F}{W} (y_1 - y_2) = K' (LMDF) \qquad (II - 1)$$

where $R_r$ = Average rate of conversion in the reactor, gm-moles/sec x gram catalyst

$F$ = hydrogen molar flow rate, gram moles/sec

$W$ = mass of catalyst in system, grams

LMDF = Log mean driving force, $(y_1-y_2) / \ln \left[(y_1-y_e)/(y_2-y_e)\right]$

$y_1$ = reactor inlet orthohydrogen mole fraction

$y_2$ = outlet orthohydrogen mole fraction

$y_e$ = equilibrium orthohydrogen mole fraction

$K'$ = effective rate constant, gm-moles/sec x gram catalyst

$$= n\pi D\, r^2 \sqrt{A} \left(\frac{\exp(2\sqrt{A}L) - 1}{\exp(2\sqrt{A}L) + 1}\right) \left(\frac{P}{RT}\right) \qquad (II - 2)$$

$n$ = number of pores per gram

$\pi$ = 3.14

D = molecular diffusivity, $cm^2/sec$

L = average pore length, cm

r = average pore radius, cm

P = pressure, atmosphere

T = temperature, °K

R = gas constant

$A = \frac{2k}{Dr} (1 + 1/K)$

k = surface reaction rate constant, $cm^3/sec \times cm^2$

K = equilibrium constant

The preliminary model had one serious drawback: the model assumed that all the pore mouths were located at the external surface of the catalyst. Since an actual catalyst particle has interconnecting pores, it becomes unrealistic to consider average pore radii and lengths. But the preliminary ideal case did lead to the evolution of a more exact model which was applicable to the ortho-parahydrogen conversion system.

## B. FINAL MODEL

The improved model is similar to a modification of the Thiele method proposed by Smith*. The latter investigators tested their model using ortho-parahydrogen conversion data and found close agreement.

The derivation begins with a mass balance for orthohydrogen on a spherical shell of thickness r with a single particle:

| Input of $O\text{-}H_2$ to the segment | - output - | amount of $O\text{-}H_2$ reacted within the segment | = | Amount of $O\text{-}H_2$ accumulation |
|---|---|---|---|---|

---

* Rao, M. R. and J. M. Smith: "Diffusion Resistances in Alumina and Silica Catalysts" AIChE Journal 9, 485 (1963)

For a steady state case, the accumulation is zero and

$$N_o\big|_{r + \Delta r} \; 4\pi(r + \Delta r)^2 - \left(N_o\big|_r\right) 4\pi r^2 - R_o (4\pi r^2 \Delta r) = 0 \qquad \text{(II - 3)}$$

In Equation (II - 3), $N_o\big|_{r + \Delta r}$ is the rate of orthohydrogen radial influx through an imaginary spherical surface at a distance $r + \Delta r$ from the center of the sphere. $R_o$ is the rate of ortho-parahydrogen conversion per unit volume of catalyst. Rearranging and allowing $\Delta r \to 0$ leads to

$$\lim_{\Delta r \to 0} \frac{(r^2 N_o)\big|_{r + \Delta r} - (r^2 N_o)\big|_r}{\Delta r} = r^2 R_o$$

$$\text{and} \quad \frac{d}{dr}(r^2 N_o) = r^2 R_o \qquad \text{(II - 4)}$$

Now, Fick's Law of Diffusion states

$$N_o = D_o \frac{dC_o}{dr} \qquad \text{(II - 5)}$$

where $C_o$ = concentration of orthohydrogen within the pellet, gm-moles/cm$^3$ gas and pellet

$D_o$ = Diffusivity of O-$H_2$ within the pellet.

Defining $\epsilon$ as the pore or gas fraction of the pellet, the orthohydrogen concentration can be expressed in terms of the gas phase mole fraction, $\epsilon$ , pressure, and temperature of the system using the perfect gas law:

$$C_o = y \left(\epsilon \frac{P}{RT}\right)$$

thus $$N_o = -D_o \epsilon \frac{P}{RT} \frac{dy}{dr}$$

In addition, $D_o$ is a diffusivity based on total area. The total area of the spherical shell of radius r consists of both solids and pores.

$D_o$ is related to a true gas phase diffusity by

$$D_o = \epsilon D$$

thus $$N_o = -(D \epsilon^2) \frac{P}{RT} \frac{dy}{dr}$$

Two kinds of diffusion in pores are possible. If the mean free path of the diffusing molecule is small with respect to the pore radius, the collisions between molecules control diffusion and the usual molecular diffusivity, $D_M$, is applicable. If the pore is small in comparison with the mean free path, collisions with the pore wall control the process. Then the Knudson diffusivity, $D_K$ is applicable.

To account for both mechanisms, one way of combining the two is

$$\frac{1}{D} = \frac{1}{D_K} + \frac{1}{D_M}$$

$$D = \frac{1}{\frac{1}{D_K} + \frac{1}{D_M}}$$

and $$D_i = \frac{\epsilon^2}{\frac{1}{D_K} + \frac{1}{D_M}} \qquad \text{(II - 6)}$$

where $D_i$ is now defined as the "effective diffusity" of orthohydrogen within the pellet, $cm^2/sec$

thus $$N_o = -D_i \frac{P}{RT} \frac{dy}{dr}$$ and

Equation II - 4 becomes

$$-\frac{d}{dr} \left(r^2 D_i \frac{P}{RT} \frac{dy}{dr}\right) = r^2 R_o \qquad \text{(II - 7)}$$

Assuming that the ortho-para transition rate, $R_o$, can be expressed as a first order, reversible reaction, and noting that the equilibrium constant for the conversion equals 1.0 at 77°K, the reaction temperature, Equation (II - 7) can be integrated using the following boundary conditions:

$y$ = bulk gas orthohydrogen mole fraction at $r = \frac{d_p}{2}$, the particle radius

$\frac{dy}{dr} = 0$ at $r = 0$

These results were used to obtain the rate of pore diffusion as a function of the bulk gas orthohydrogen mole fraction. A macroscopic material balance, identical to that presented in Appendix I, was applied and the final result was the following expression for the rate of reaction when pore diffusion and surface reaction controlled the over-all conversion:

$$R_r = \frac{F}{W}(y_1 - y_2) = k E_p \text{ (LMDF)} \qquad \text{(II - 8)}$$

where $R_r$ = Observed rate of conversion, gm moles/sec x gram catalyst

$k$ = specific reaction constant, gm moles / sec x gm catalyst

$$E_p = 3\left(\frac{h \coth h - 1}{h^2}\right)$$

$$h = \frac{d_p}{2}\sqrt{\frac{k \rho_p RT}{D_i P}}$$

$\rho_p$ = particle density, $gm/cm^3$

# APPENDIX III

## PORE MOUTH CONTAMINATION THEORY

In conjunction with the experimental investigation of the effect of adsorbed nitrogen on the activity of ortho-para catalysts, Air Products and Chemicals, Inc. performed a theoretical analysis of this phenomenon in light of the results of prior studies of mass transfer resistance.

### A. DERIVATION OF THEORY

The analysis assumed that all of the nitrogen was adsorbed in a monolayer just within the pore mouths. This adsorption would decrease the area available for catalysis, decrease the free cross sectional area of the pores, and greatly decrease the reactant concentration gradient within the pores. All of these would, in turn, decrease the rates of pore gas phase diffusion and surface reaction, and thus lower the catalyst activity. The analysis presented here accounts only for the decrease in catalytic area and the decrease in driving force, and the final result is a relationship between the fraction of the surface contaminated and the decrease in catalytic activity. The model is presented pictorially in Figure III - 1.

Define $\alpha$ as the fraction of surface covered by the nitrogen monolayer, and f as the fraction of initial catalytic activity remaining after a surface coverage of $\alpha$ .

$$f = \frac{\text{reaction rate after nitrogen adsorption, gm-moles/gram cat. x sec}}{\text{initial reaction rate, gram-moles/gm cat. x sec}}$$

$$f = \frac{R'}{R} \qquad \text{(III - 1)}$$

#### 1. Initial Reaction Rate

At 77°K, the equilibrium constant for the ortho-parahydrogen is equal to 1.0, and thus the equilibrium mole fraction of orthohydrogen, $y_e$, is 0.5. For this case, the first order, reversible reaction can be represented by the simplified equation.

$$R_r = k_W E_p (y - y_e) \qquad \text{(III - 2)}$$

where

$R_r$ = Conversion rate, gm moles/sec x gm-cat.

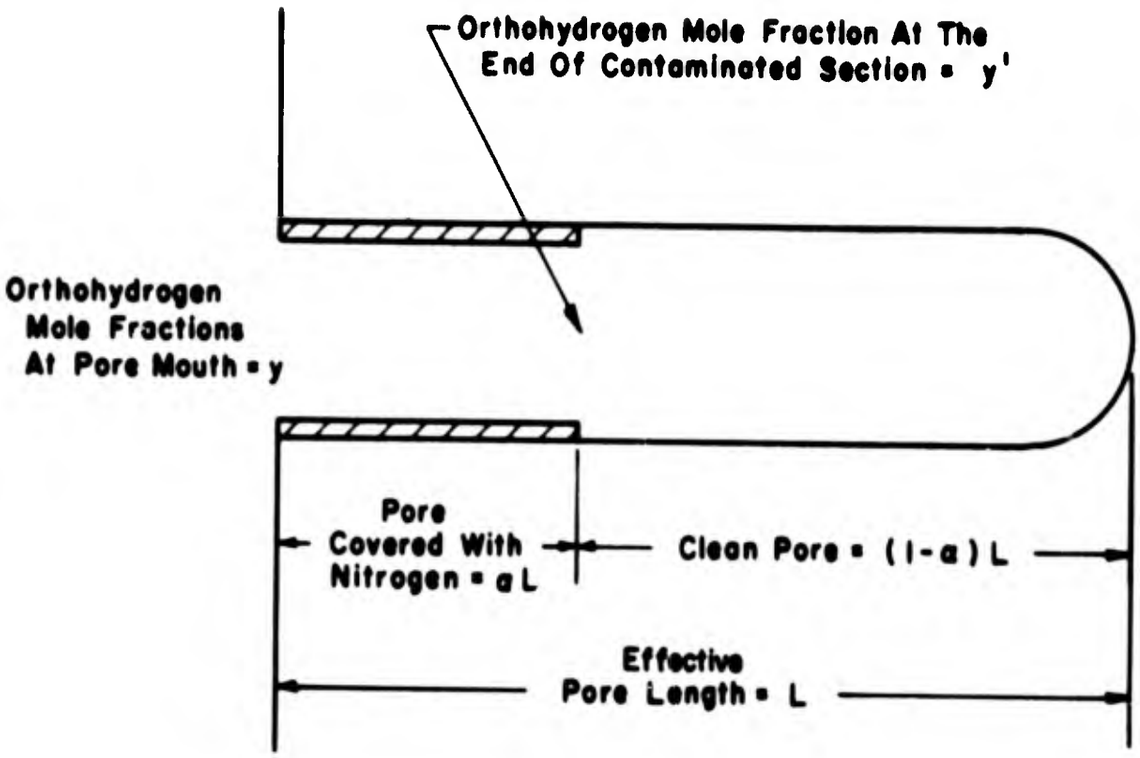


Figure III-1. Pore Mouth Contamination Theory Model Pore

$k_W$ = first order reaction rate constant, gm moles/gm cat x sec

$E_P$ = pore diffusion effectiveness factor

$$= 3 \left( \frac{h \coth h - 1}{h^2} \right)$$

$$h = X \sqrt{\frac{k_W \rho_p RT}{D_i P}}$$

$X$ = catalyst pore length, cm

$\rho_p$ = catalyst particle density, grams/cm$^3$

$P$ = pressure, atmospheres

$T$ = temperature, °K

$R$ = gas constant, atm x cm$^3$/gm mole x°K

$D_i$ = effective pore diffusivity, cm$^2$/sec

2. Nitrogen Adsorption Case

When the fraction of the pore, $\alpha X$, nearest the mouth becomes covered with a monolayer of nitrogen, the rate of reaction in that pore is reduced to

$$R'_r = k_W' E_P' (y' - y_e) \qquad \text{(III - 3)}$$

where $y'$ = orthohydrogen mole fraction at $\alpha X$, the end of the nitrogen covered portion of the pore

Remember, $k_W$ and $k_W'$ are based on a unit mass of catalyst. Both the clean and contaminated catalysts have the same chemical compositions and total surface areas. However, the catalytically-effective surface area of the latter has been reduced by a fraction, $\alpha$. Thus the relationship between the two is

$$\frac{k_W}{A} = \frac{k_W'}{A'}$$

where A and A' are the effective specific surface areas, $cm^2/gm$

$$A' = A(1-\alpha)$$

and $$k_W' = (1-\alpha)\, k_W \qquad \text{(III - 4)}$$

In the same manner:

$$E_P' = 3\,\frac{h' \coth h' - 1}{(h')^2}$$

$$h' = X' \sqrt{\frac{k_W'\, \rho_P\, RT}{D_i\, P}}$$

Neglecting the effect of the reduction of the pore mouth cross sectional area due to $N_2$ adsorption:

$$D_i' = D_i$$

$$X' = (1-\alpha)\, X$$

$$k_W' = (1-\alpha)\, k_W$$

and

$$h' = (1-\alpha)\, X \sqrt{\frac{(1-\alpha)\, k_W\, \rho RT}{D_i\, P}}$$

$$h' = (1-\alpha)^{3/2} h$$

$$E'_P = 3\,\frac{(1-\alpha)^{3/2} h \coth (1-\alpha)^{3/2} h) - 1}{(1-\alpha)^2 h^2} \qquad \text{(III - 5)}$$

It can be seen that

rate of reaction within the pores = rate of diffusion into the pore mouths

Rate of diffusion into the pore mouths $= D_i\, S\, \frac{P}{RT} \left(\frac{dy}{dx}\right)_{x=0}$ (III - 6)

where

$\left(\frac{dy}{dx}\right)_{x=0}$ = orthohydrogen gradient at pore mouths, $cm^{-1}$

P = pressure, atm

T = temperature, °K

R = Gas constant, atm x $cm^3$/°K x gm mole

$D_1$ = effective pore diffusivity, $cm^2$/sec

S = external catalyst surface, $cm^2$/gram

$= \frac{6(1-\epsilon_v)}{d_p \rho_B}$

$\epsilon_v$ = void fraction of catalyst bed

$d_p$ = particle diameter, cm

$\rho_B$ = bulk density of catalyst bed, grams/$cm^3$

By a material balance, it can be shown that the orthohydrogen gradient in the $N_2$ covered pore mouth section is linear:

$$\left.\frac{dy}{dx}\right|_{x=0} = \frac{y - y'}{0 - \alpha x} = -\frac{y - y'}{\alpha x}$$

Making the above substitutions into Equations (III - 3) and (III - 6) and equating these expressions leads to:

$$\frac{D_1 (1-\epsilon_v) P}{x \rho_B RT}\left[\frac{y - y'}{\alpha x}\right] = k_W \frac{(1-\alpha)^{3/2} h \coth\left[(1-\alpha)^{3/2} h\right] - 1}{(1-\alpha)^2 h^2} (y' - y_e) \qquad \text{(III - 7)}$$

Solving the above equation for y', substituting this value into Equation (III - 3), and in turn using this expression for the $R_r'$, the reaction rate after nitrogen adsorption, and $R_r$, the initial reaction rate, the fractional decrease in reaction rate in terms of nitrogen coverage becomes:

$$f = \frac{1}{3}\left[\frac{\dfrac{(1-\epsilon_v)\,D_i\,P}{\alpha(1-\alpha)^2\,X^2\rho_B\,RT}}{\dfrac{D_i(1-\epsilon_v)\,P}{\alpha X^2\rho_B\,RT} + \dfrac{k_W}{(1-\alpha)^2h^2}\left[(1-\alpha)^{3/2}h\coth\left\{(1-\alpha)^{3/2}h\right\}-1\right]}\right]$$

$$\left[\frac{(1-\alpha)^{3/2}\,h\coth\left\{(1-\alpha)^{3/2}\,h\right\}-1}{h\coth h-1}\right] \qquad \text{(III - 8)}$$

## B. APPLICATION OF THEORY

Using the known catalyst characteristics of APACHI 1049-100, the above theory was applied to the problem of nitrogen adsorption on APACHI catalysts.

APACHI 1049-100, 30-50 mesh, chemical and physical characteristics:

$P$ = 100 psia

$T$ = 77°K

$k_W$ = 0.0292 grams moles $H_2$/sec x gram catalyst

$h$ = $1.41 \times 10^2$ X

$X$ = 0.0248 cm

$D_i$ = $6.85 \times 10^{-4}$ $cm^2$/sec

$\epsilon_v$ = 0.167

$\rho_B$ = 0.48 gm/$cm^3$

With these data, the following values of f were calculated as functions of $\alpha$ :

| $\alpha$ | f |
|---|---|
| 0.05 | 0.320 |
| 0.10 | 0.270 |
| 0.20 | 0.221 |
| 0.40 | 0.151 |

These theoretical results are compared to the experimental results in Figure 24 on Page 60.